Upper Ocean Stratification in the Eastern Pacific during the SPURS-2 Field Campaign

S. Katsura[1], J. Sprintall[1], and F. M. Bingham[2]

[1] Scripps Institution of Oceanography, University of California, San Diego, La Jolla.

[2] Center for Marine Science, University of North Carolina Wilmington, Wilmington, North Carolina.

Corresponding author: Shota Katsura (skatsura@ucsd.edu)

Key Points:

- In the eastern tropical Pacific, barrier layers were thickest in the salinity front and temperature inversions warmest in the fresh pool.
- Ekman and geostrophic flow form barrier layers and temperature inversions by tilting of salinity fronts on synoptic spatio-temporal scales.
- Tilting of salinity fronts occurs only intermittently resulting in a patchy distribution of barrier layer formation in the eastern Pacific.

Abstract

The region between a shallow mixed layer and a deep isothermal layer resulting from salinity stratification is called a barrier layer (BL). Since BLs hinder the surface heat and momentum exchange with the ocean subsurface, they play an important role in air-sea interaction. Synoptic features and formation of BLs and associated temperature inversions (TIs) in the Eastern Pacific Fresh Pool (EPFP) were investigated using shipboard observations. BLs and TIs were found in the high precipitation EPFP, a frontal transition zone (FTZ) and in the sea surface salinity (SSS) front during a 2016 boreal summer cruise. During a 2017 boreal autumn cruise, BLs and TIs were found from the southern part of the EPFP to the SSS front. The BLs in the SSS front and the FTZ were meridionally displaced from the precipitation maximum during both the 2016 and 2017 cruises. Freshening and cooling by tilting of both the isohalines and isotherms of the SSS front occurred via Ekman and geostrophic flow during both cruises, and also within the EPFP during 2016. The SSS front was a dominant contributor to the density gradient in the horizontal plane. A high dissolved oxygen content observed within BLs confirmed that the surface flow plays an important role in the BL and TI formation through the tilting process. Patchy distribution of freshening and cooling by tilting implies an intermittent BL and TI formation with short time scales.

Plain Language Summary

In some regions of the ocean surface layer, the base of a density-defined mixed layer is shallower than that of a temperature-defined isothermal layer due to a strong salinity stratification. The region between the base of the mixed layer and the isothermal layer is called a barrier layer (BL). The BL acts as a barrier to heat and momentum exchange between the surface and subsurface ocean and may have an important role in air-sea interaction. When BLs contain temperature inversions (TIs) of water warmer than the sea surface, they can work to increase sea surface temperature being entrained into the overlying surface mixed layer and hence have a significant impact. Based on shipboard observations, wind-driven Ekman flow and geostrophic flow caused surface freshening and cooling that contributed to the formation of BLs and TIs in the Eastern Pacific Fresh Pool. The role of the surface flows contributing to the BL and TI formation were supported by the horizontal structure of the observed salinity, temperature and oxygen profiles. However, the freshening and cooling of the BLs and TIs showed a patchy distribution suggesting their formation occurs intermittently.

1 Introduction

Sea surface salinity (SSS) in the eastern tropical Pacific is minimum in the Eastern Pacific Fresh Pool (EPFP) where the mean SSS is lower than 34.0 (Fig. 1). The EPFP has mean SSS < 33.5 between 5°−15°N and east of 130°W resulting from precipitation associated with the intra-American monsoon system (Amador et al., 2006) and westward transport of water vapor across the Panama isthmus (Benway and Mix, 2004). The EPFP extends westward and forms a zonal band of low SSS (< 34.0) along ~10°N likely related to high precipitation due to the Intertropical Convergence Zone (ITCZ) and/or westward advection by the North Equatorial Current (NEC). The EPFP roughly aligns with the eastern Pacific warm pool adjacent to the central American isthmus, where sea surface temperature (SST) is > 28℃ (Fig.1). A seasonal cycle in SSS is evident in the horizontal extent of the EPFP and is controlled by a combination of freshwater flux, horizontal advection, and vertical mixing (Delcroix and Hénin, 1991; Fiedler and Talley, 2006; Alory et al., 2012; Yu, 2014; Melnichenko et al., 2019). The western edge of

the EPFP also migrates interannually in association with precipitation anomalies related to the El Niño-Southern Oscillation (ENSO; Guimbard et al., 2017). The SSS front south of the EPFP separates the fresher water induced by the ITCZ precipitation to the north from the saltier water to the south (Yu, 2014, 2015; Kao and Lagerloef, 2015). Seasonality in the meridional migration and intensity of the SSS front couples with the EPFP via the wind field and Ekman processes (Yu, 2015). Considering that salinity is an important indicator of the freshwater flux between the ocean and atmosphere (Schmitt, 2008; Lagerloef et al., 2010) and that heavy rainfall associated with the ITCZ is a major source of freshwater input to the ocean (Waliser and Gautier, 1993; Yu et al., 2015), knowledge of the salinity structure and variability in the eastern tropical Pacific is important for a better understanding of the hydrological cycle. Indeed, a few recent studies have linked SSS variability to terrestrial rainfall (e.g. L. Li et al., 2016a; 2016b; Rathore et al, 2020) although it remains unclear on the mechanisms that might result in such a statistical correspondence.

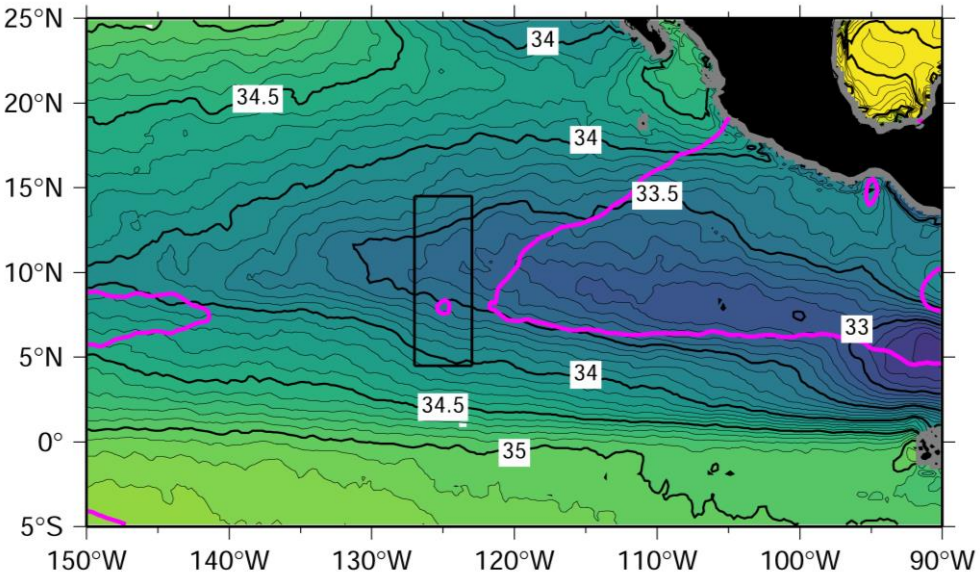

Figure 1. Distribution of mean sea surface salinity in 2016−2017 from SMAP. The rectangle indicates the region of the SPURS-2 field campaign (see Figure 3). Magenta lines indicate the mean surface temperature isotherms of 28°C in 2016−2017 from OISST.

Throughout much of the world oceans, temperature controls mixed layer depth (MLD), although in some regions salinity stratification is important. When the density-stratified mixed layer is shallower than the thermally-stratified isothermal layer, the salinity stratified region in between is called a barrier layer (BL; Fig. 2). BLs can reduce the cooling effect of entrainment because the entrained water has almost the same temperature as the overlying mixed layer (e.g., Godfrey and Lindstrom, 1989; Vialard and Delecluse, 1998; Yan et al., 2017; Pujiana and McPhaden, 2018). When a BL is associated with a vertical temperature inversion (TI; Fig. 2) that contains warmer water than the surface mixed layer above, the entrainment effect can even warm the mixed layer. BLs also trap momentum flux from the atmosphere to the ocean and can result in accelerated flow within a shallower near-surface layer (Roemmich et al., 1994; Vialard and Delecluse, 1998). For all these effects, the BL is an important factor in air-sea interaction and offers a potential mechanism for linking the salinity stratification to the hydrological water cycle (e.g., Drushka et al., 2014; Y. Li et al., 2017a; 2017b).

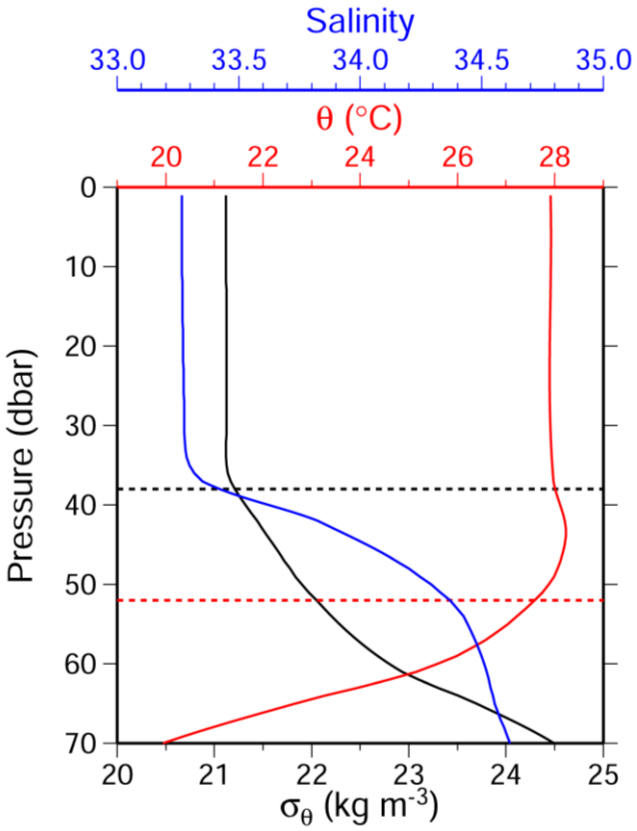

Figure 2. Vertical profiles of salinity (blue), temperature (red), and σ_θ (black) observed by an underway Conductivity-Temperature-Depth (uCTD) profiler at 9.771°N, 234.833°W on 26 Oct 2017. Horizontal dashed black and red lines indicate the MLD and ILD, respectively. In this case, the barrier layer (ILD - MLD) is 14 dbar thick.

A seasonal climatological study of BLs and TIs based on Argo profiling float data by Katsura and Sprintall (2020; henceforth KS2020) revealed that BLs are distributed along the SSS front south of the EPFP with a seasonal peak in boreal summer and autumn. Bingham et al. (2020) show an example of this from a high-resolution model. BLs in the SSS front tend to be associated with TIs within the gap between the eastern and western warm pools (see Fig. 1) in boreal autumn. KS2020 further clarified that southward Ekman advection across the SSS front driven by eastward wind works to both freshen and cool the surface layer and contributes to the formation of BLs with TIs through the tilting of the SSS front in boreal summer and autumn. The SSS front is the dominant contributor to the horizontal density gradient and compensates the horizontal temperature gradient, which make BL and TI formation possible through tilting processes (Cronin and McPhaden, 2002). Precipitation was a secondary contributor to BL formation in autumn although it contributed to the broader distribution of BLs within the EPFP in summer (KS2020). Considering the extremely shallow mixed layer in this eastern Pacific region (Suga et al., 2004; Fiedler and Talley, 2006), BLs and associated TIs can have a significant impact on SST and the heat budget of the overlying mixed layer and in the evolution of ENSO (e.g., Maes et al., 2002; 2005). Nonetheless, the Argo data used in KS2020 permit investigation of BLs and TIs only on monthly-time scales, even though both BLs and TIs may be much shorter lived. In addition, BLs determined from individual profiles are known to exhibit more uneven or “patchy” distribution compared to the fairly continuous distribution in spatial

extent and seasonality evident in monthly climatological studies such as KS2020 (Sato et al., 2004; 2006; Mignot et al., 2009). Patchiness in BL presence or BL thickness in a region will potentially degrade the impact of the role that BLs play in air-sea interaction. If the spatial gaps between BL presence are large or "porous" (Mignot et al., 2009) then the ability of BLs to reduce heat exchange will likely be much diminished, potentially permitting the maintenance of normal entrainment processes in the region.

The Salinity Processes in the Upper-ocean Regional Study 2 (SPURS-2) was a multiyear field program to study the upper-ocean salinity structure and understand the physical processes controlling the salinity balance in the precipitation-dominated eastern tropical Pacific (Lindstrom et al., 2019). The focus area of SPURS-2 was around 10°N, 125°W in the western part of the EPFP. Shipboard surveys on the *R/V Roger Revelle* were conducted in this area in August−September 2016 and again in October−November 2017 (Fig. 1). During these two cruises, concurrent observations of both the ocean and atmosphere were conducted at high spatial resolution from various platforms (Bingham et al., 2019). The period of these two cruises corresponds to the seasonal peak of BLs and TIs in boreal summer and autumn (KS2020), and indeed, BLs with TIs were detected during the SPURS-2 cruise (Sprintall, 2019).

The purpose of this study is to investigate the distribution and formation of the BLs and TIs during the SPURS-2 cruises. Here we take advantage of the high spatial resolution and synoptic concurrent measurements collected during SPURS-2 to better understand the upper ocean stratification on shorter space and time scales compared to the climatological study of KS2020. The high horizontal along-track resolution from the meridional transects of hydrographic observations collected during the SPURS-2 cruises cannot be achieved by Argo profiling floats, such as employed in the KS2020 study. In addition, repeat surveys along the same meridional transect during both SPURS-2 cruises enables us to investigate more detailed "synoptic" features of BLs and TIs, their patchiness in distribution, as well as determine their relationship to the concurrent background hydrography and circulation. The data and methods are described in Section 2. The distribution of BLs and TIs, their relationship to the background hydrography and formation mechanisms are explored in Section 3. Finally, the synoptic features and formation of BLs and TIs detected in the SPURS-2 cruises are summarized and discussed in Section 4.

2 Data and Methods

In this study, we use vertical profiles of the upper ocean from an underway Conductivity-Temperature-Depth (uCTD) and a shipboard CTD-O_2 system collected during the two SPURS-2 cruises on the *R/V Roger Revelle* (Fig. 3). The first cruise in boreal summer from 21 August to 12 September 2016 collected 259 uCTD profiles and 50 CTD profiles. The second cruise in boreal autumn from 21 October to 11 November 2017 collected 493 uCTD profiles and 8 CTD profiles.

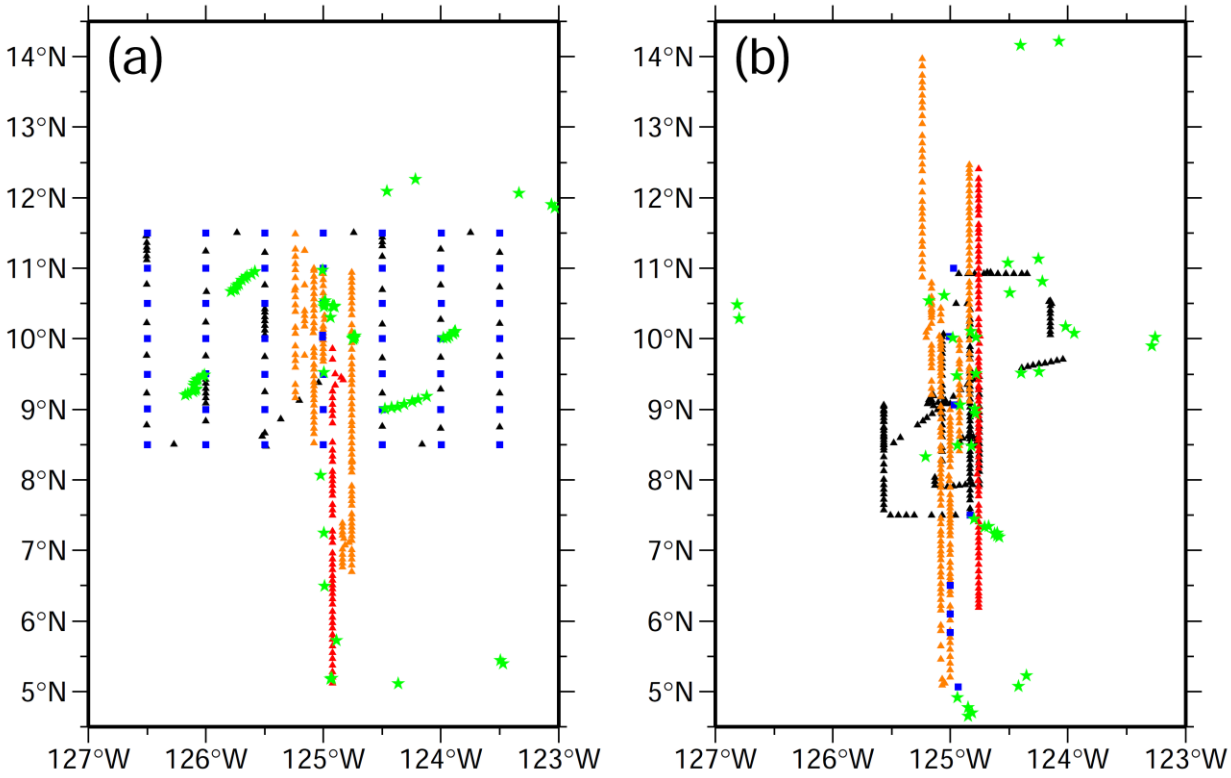

Figure 3. Location of uCTD (black, orange, and red triangles), CTD (blue squares), and Argo profiles (green stars) during SPURS-2 (a) 2016 boreal summer cruise (21 August−12 September 2016) and (b) 2017 boreal autumn cruise (21 October−11 November 2017). Orange and red triangles indicate uCTD profiles along 125°W, which are slightly shifted zonally for visibility. Red triangles in (a) and (b) indicate uCTD profiles used for Figures 5 and 7, respectively.

Measurements of temperature and conductivity (and thus salinity) from 6−400 m were obtained using the uCTD profiler. The observations were post-processed to remove salinity spikes following Ullman and Hebert (2014) and then interpolated to a 1-dbar vertical resolution using an Akima spline (Akima, 1970). Potential temperature (θ) and density (σ_θ) were then calculated. In each cruise, seven meridional transects of uCTD casts were conducted along 125°W at a ~0.1° latitude horizontal spacing (Fig. 3) which corresponds to ~30-minute or ~1-hour temporal intervals depending on the ship speed along-track. Additional uCTD casts were located within the general SPURS-2 region (Fig. 3).

The temperature, salinity, pressure, and dissolved oxygen profiles from 0−1000 dbar were obtained using the on-station shipboard CTD-O_2 system. The observations were vertically averaged to a 2-dbar interval and θ and σ_θ were calculated for each profile. During the 2016 cruise, the 50 CTD profiles were collected in a grid-like pattern with a horizontal resolution of 0.5° latitude × 0.5° longitude (Fig. 3a). During the 2017 cruise, 8 CTD casts were conducted along ~125°W (Fig. 3b).

Temperature and salinity profiles from Argo profiling floats were also available during each SPURS-2 cruise period (Fig. 3) and were obtained from the advanced automatic QC Argo data version 1.2. from the Japan Agency for Marine-Earth Science and Technology and were quality checked as outlined by Oka et al. (2007). The temperature and salinity profiles were

vertically interpolated to a 1-dbar interval using an Akima spline, and θ and σ_θ were subsequently calculated.

Current velocity profiles were measured underway from the ship's hull via acoustic Doppler current profiler (ADCP) during the two SPURS-2 cruises. Specifically, here we use the shipboard data from an Ocean Surveyor narrowband 150 kHz system that measured currents from ~17 m to ~300 m depth at a vertical resolution of 8 m. The ADCP velocity data were quality controlled and processed using the University of Hawaii UHDAS software system, and vertically interpolated to a 1-dbar interval using an Akima spline.

Shipboard *in situ* air-sea flux state variables (e.g., SST, air temperature, wind etc.), and rainfall (e.g. optical and manual rain gauges) measurements are also available during both SPURS-2 cruises (Clayson et al., 2019). The 10-m values of wind speed and the bulk fluxes of wind stress (corrected for ocean current using the near-surface ADCP velocity from the uppermost bin) were computed using the COARE 3.5 algorithm (Fairall et al., 2003; Edson et al., 2013).

SSS and SST were from the daily L3 8-day running mean 70-km version-4.0 product of the National Aeronautics and Space Administration (NASA) Soil Moisture Active Passive (SMAP; Meissner and Wentz, 2018) and from the Advanced Very High Resolution Radiometer daily product of Optimum Interpolation Sea Surface Temperature (OISST; Reynolds et al., 2007), respectively. The horizontal resolution of these gridded data is 0.25° latitude × 0.25° longitude.

Precipitation was from the NASA Integrated Multi-satellitE Retrievals for GPM (IMERG) version 4.0, a merged satellite product available from 2014 every 30 min at 0.1° latitude × 0.1° longitude horizontal resolution (Kummerow, 1998). IMERG is meant to provide an improved rainfall product over the remotely sensed Tropical Rainfall Measuring Mission (TRMM) that is based on a single sensor (Skofronick-Jackson et al., 2017).

Isothermal layer depth (ILD) was defined as the depth at which θ decreases by 0.2°C from 10-dbar depth (de Boyer Montégut et al., 2007). MLD was defined as the depth at which σ_θ increases from 10-dbar depth by the equivalent value to a temperature decrease of 0.2°C at 10-dbar salinity (Sprintall and Tomczak, 1992). Barrier layer thickness (BLT) was defined as the difference between the ILD and MLD when that difference is greater than zero. The amplitude of the temperature inversion associated with any BL ($\Delta\theta$) was defined as the difference between the temperature at the vertical temperature maximum within the BL minus the temperature at the MLD (KS2020). Following previous studies, we only considered BLs with BLT > 10 dbar and TIs with $\Delta\theta$ > 0.1°C (e.g., Sato et al., 2004; 2006; KS2020). This does not mean BLs with 0 < BLT < 10 dbar are not important because in some regions even thin BLs have been shown to interfere with the cooling effect of entrainment and modify the heat budget of overlying mixed layer (Drushka et al., 2014). Rather, in our study we are more interested in understanding the conditions that might lead to BL and TI formation, as well as being mindful about the vertical resolution of the data in determining BLT. For the 2016 and 2017 cruises, 36.0% and 26.2% of all profiles were found to have non-zero BLT < 10 dbar, respectively.

For each of the uCTD transects along 125°W during the two SPURS-2 cruises, we defined three regions: the SSS front, the frontal transition zone (FTZ), and the EPFP. Mean SSS in the EPFP was 32.95 during the 2016 summer cruise compared to 33.41 during the 2017 autumn cruise reflecting the seasonality of the region, so SSS was not necessarily a good

criterion to define the EPFP during both cruises. Alternatively, we found that $\partial SSS/\partial y$ clearly separated the EPFP from the SSS frontal region. The boundary between the SSS front and the FTZ was best defined as the location where $\partial SSS/\partial y < -10 \times 10^{-6}$ m^{-1}. The SSS front was then defined as the region to the south of that boundary. The FTZ was defined as the region between this boundary and a change of 0.5° in latitude to the north. The EPFP was then defined as the region north of the northern edge of the FTZ. When an SSS front was not detected in a transect based on this criterion, all of the profiles in the transect were assumed to be within the EPFP. The boundary was detected in 3 transects in each cruise, and the mean latitude during the 2016 and 2017 cruises was 7.18°N ± 0.03° and 7.06°N ± 0.57°, respectively.

3 Results

3.1 Hydrography and Distribution of BLs and TIs during SPURS-2 Field Campaign

The mean distribution of SSS during the 2016 boreal summer cruise showed a zonal band of low SSS (< 33.0) at 8°−11°N (Fig. 4a) with SSS increasing to the south. North of 11°N, SSS lower than 33.0 was found west of 126°W, and SSS higher than 33.0 extended northeastward from 11°N, 126°W. The distribution of mean SST in the 2016 summer cruise mirrored the mean SSS distribution (Fig. 4b); high SST corresponding with low SSS. A zonal band of high SST > 28.5℃ was found at 8°−11°N, corresponding to the zonal band of low SSS, and SST decreased to the south. SST lower than 28.5℃ extended eastward from 11°N, 126.5°W, with SST higher than 28.5℃ found to the north. During the 2016 summer cruise, northeastward winds prevailed north of 8.5°N and near calm winds south of 8.5°N (Fig. 4c), corresponding to the expected seasonality of the regional wind field in the eastern Pacific (Guimbard et al., 2017; KS2020). The eastward flowing North Equatorial Countercurrent (NECC) was evident near 7°N in the near-surface with speeds < 0.5 m s^{-1} during the 2016 summer cruise (Fig. 4d). Occasional weak westward currents and small-scale perturbations were detected along the 125°W section.

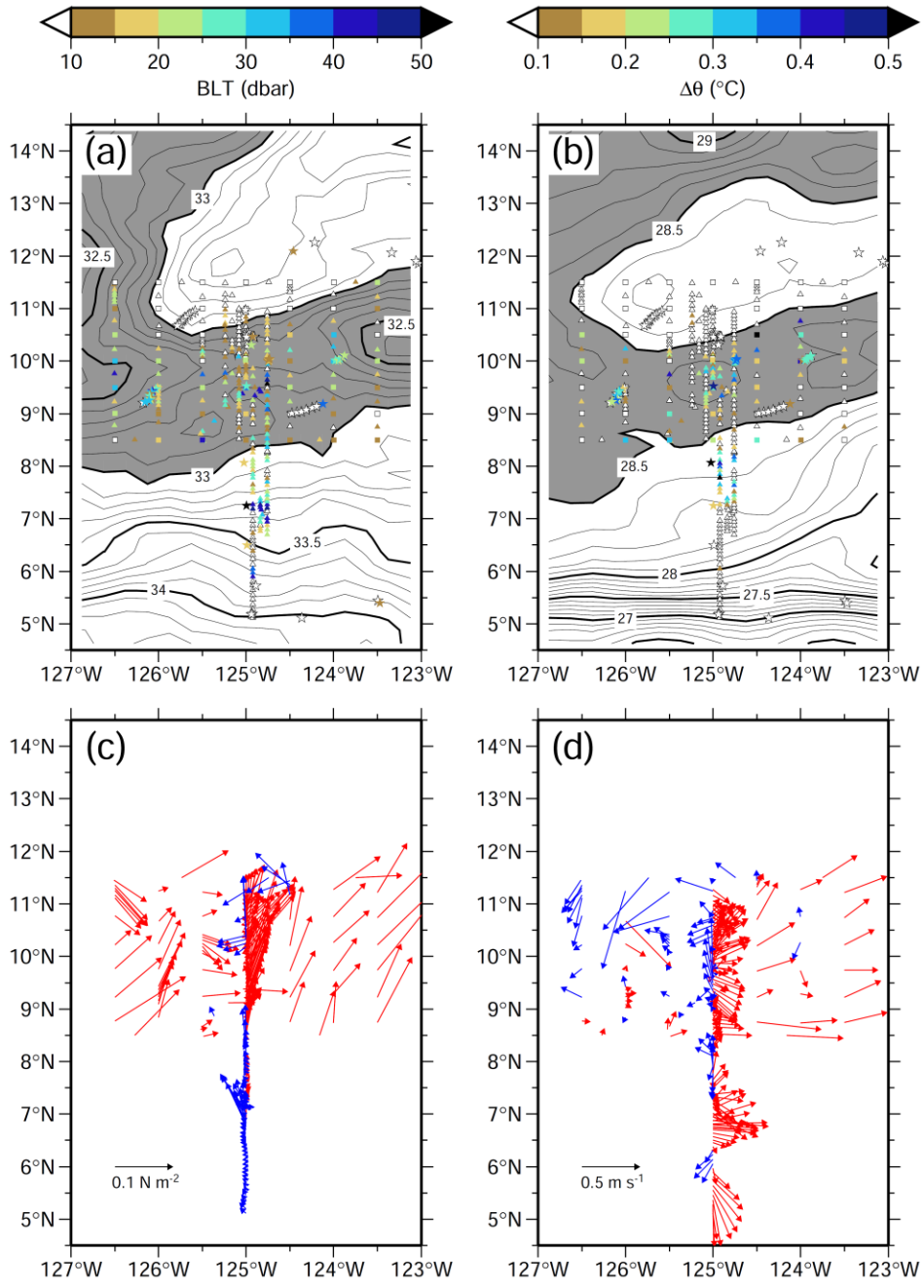

Figure 4. Distribution of (a) BLT (dbar) and (b) $\Delta\theta$ (°C) from uCTD casts (triangles), CTD casts (squares), and Argo profiling floats (stars) during SPURS-2 2016 cruise. Triangles along 125°W are slightly shifted zonally to improve visibility. Contours indicate (a) the mean SSS from SMAP and (b) the mean SST from OISST (°C) from 21 August to 12 September 2016. Gray shading indicates (a) SSS lower than 33.0 and (b) SST higher than 28.5°C. Distribution of (c) wind stress (N m^{-2}) and (d) near-surface current (m s^{-1}) during the SPURS-2 2016 cruise, averaged 1-hour prior and posterior to the time of uCTD and CTD profiles. Red and blue arrows in (c) and (d) indicate eastward and westward direction, respectively.

During the 2016 boreal summer cruise, BLs with TIs were detected in all three regimes, albeit with different characteristics: BLs within the SSS front were thicker than in the EPFP and

FTZ, while BLs within the EPFP showed a more coherent distribution. TIs were less frequent in the SSS front compared to the FTZ and the EPFP. The BL presence north of 8.5°N in the EPFP corresponded to where the mean SSS was < 33.0 (Fig. 4a). These BLs tended to be associated with the TIs in the zonal band where the mean SST > 28.5℃ (Fig. 4b).

The temperature and salinity profiles captured during the longest transect along 125°W (Fig. 5) are largely representative of the profiles from the other six transects during the 2016 cruise. The ILD was around 55 dbar while MLD ranged from 15−50 dbar in the EPFP and FTZ, resulting in BLs with 10−40 dbar thickness. In the SSS frontal region, thick BLs > 35 dbar were associated with the southern edge of an isolated warm, fresh region at around 6°N but otherwise were practically non-existent. TIs were observed in the EPFP where the temperature within isothermal layers was warmer than 28.5℃ (Fig. 5b) and were warmest just north of the FTZ.

For all meridional transects along 125°W during the 2016 cruise, the mean BLT in the SSS frontal regime was 29.22 dbar and 28.71 dbar in the FTZ, thicker than in the EPFP at 20.29 dbar, although there was little statistical difference between the mean BLT across all regimes (Table 1). The mean $\Delta\theta$ in the SSS front was nearly half the amplitude of the $\Delta\theta$ in the EPFP and FTZ. The frequency of BLs and TIs in the FTZ was 100% and 85.7%, respectively, compared to only 64.9% (43.9%) of profiles with BLs and 37.3% (2.4%) of profiles with TIs in the EPFP (SSS front).

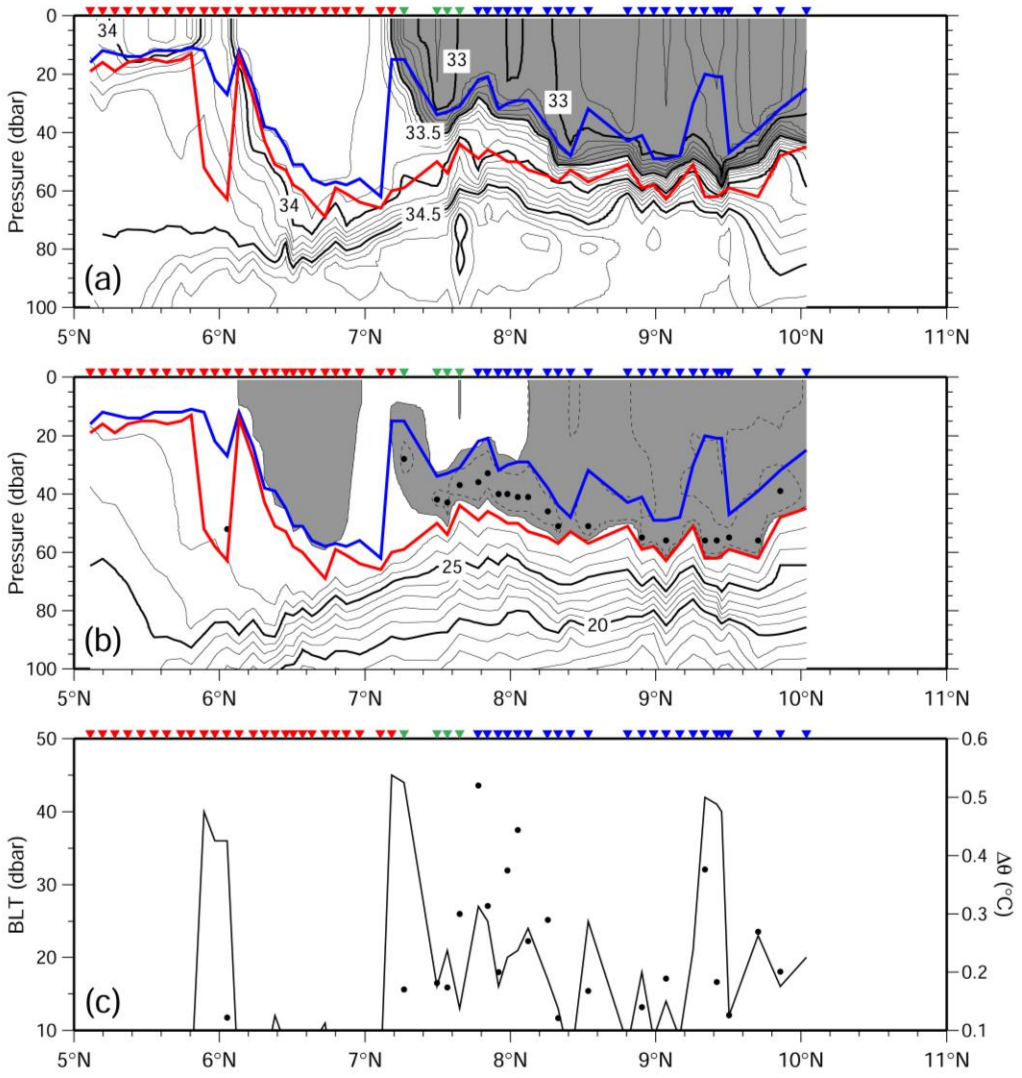

Figure 5. Meridional transects of (a) salinity and (b) θ (°C), and (c) distribution of BLT (dbar; line) and $\Delta\theta$ (°C; dots) along 125°W from uCTD profiles observed during 8−10 September 2016 (red triangles in Figure 2a). Inverted triangles at the top of each panel indicate the locations of uCTD profiles in the EPFP (blue), the FTZ (green), and the SSS front (red). Gray shading in (a) and (b) indicates salinity lower than 33.5 and θ higher than 28°C, respectively, and blue and red curves indicate the MLD and ILD, respectively. Dashed contours in (b) denote θ = 28.2°C. Black dots in (b) denote the depth of the vertical temperature maximum where $\Delta\theta$ > 0.1°C.

		MLD (dbar)	ILD (dbar)	BLT (dbar)	$\Delta\theta$ (°C)	Number of Profile	Number of Profile with BL and Frequency	Number of Profile with TI and Frequency
2016	EPFP	29.50 (1.72)	44.21 (2.23)	20.29 (2.02)	0.233 (0.026)	134	87 (64.9%)	50 (37.3%)
	FTZ	24.71 (3.97)	53.43 (2.78)	28.71 (6.17)	0.224 (0.046)	14	14 (100.0%)	12 (85.7%)
	SSS front	26.02 (5.10)	41.27 (5.77)	29.22 (5.16)	0.122 (-)	41	18 (43.9%)	1 (2.4%)
2017	EPFP	25.35 (1.03)	44.46 (2.15)	30.22 (2.61)	0.188 (0.017)	226	130 (57.5%)	63 (27.9%)
	FTZ	18.78 (2.58)	58.17 (3.23)	39.39 (3.31)	0.149 (0.015)	18	18 (100.0%)	11 (61.1%)
	SSS front	37.55 (4.89)	64.08 (5.37)	32.14 (5.79)	0.147 (0.020)	53	42 (79.2%)	12 (22.6%)

Table 1. Mean values of MLD (dbar), ILD (dbar), BLT (dbar) and magnitude of $\Delta\theta$ (°C) and the number of profiles in the EPFP, the FTZ, and the SSS front along the 125°W transects during the 2016 and 2017 cruises. Values in the parentheses indicates the 95% confidence interval. Calculation of mean BLT and mean $\Delta\theta$ was performed for all uCTD profiles with BLT > 10 dbar and $\Delta\theta > 0.1$°C, respectively. Frequency of profiles with BLs and TIs were relative to the total number of profiles in each regime.

Mean SSS during the 2017 boreal autumn cruise was saltier compared to the 2016 boreal summer cruise. The EPFP region, where SSS < 33.5, was restricted to 7.5°−12.5°N, with minimum SSS < 33.0 found between 8.5°−10.5°N east of 125.5°W (Fig. 6a). The SSS front south of the low SSS between 6.5°−8.5°N was sharper than in the 2016 boreal summer cruise (Figs. 4a and 6a). The mean SST during the 2017 cruise had a meridional maximum (SST > 28.2°C) in the northern part of the SPURS-2 region between 11°−14.5°N (Fig. 6b) that did not coincide with the location of the SSS minimum (Fig. 6a). Southwestward winds prevailed north of 9.5°N with northwestward trades to the south, meridionally converging from 8°−11°N (Fig. 6c). The eastward NECC was dominant south of 11.5°N during the 2017 cruise and much stronger and more well defined compared to the 2016 cruise (Fig. 6d). The near-surface westward flowing NEC was restricted to north of 12°N.

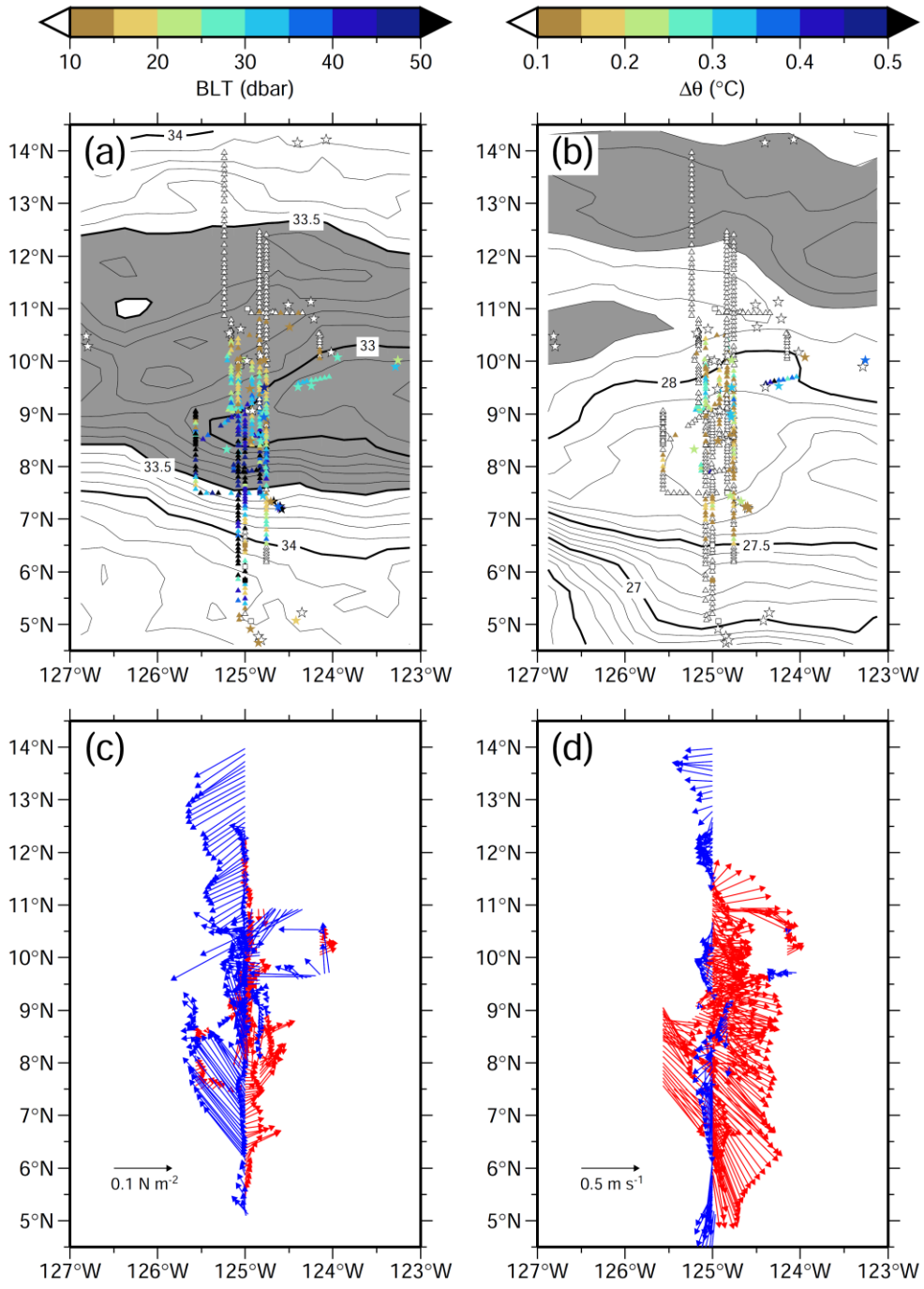

Figure 6. Distribution of (a) BLT (dbar) and (b) $\Delta\theta$ (°C) from uCTD casts (triangles), CTD casts (squares), and Argo profiling floats (stars) during SPURS-2 2017 cruise. Triangles along 125°W are slightly shifted zonally to improve visibility. Contours indicate (a) the mean SSS from SMAP and (b) the mean SST from OISST (°C) from 21 October to 11 November 2017. Gray shading indicates (a) SSS lower than 33.5 and (b) SST higher than 28.2°C. Distribution of (c) wind stress (N m^{-2}) and (d) near-surface current (m s^{-1}) during the SPURS-2 2017 cruise, averaged 1-hour prior and posterior to the time of uCTD and CTD profiles. Red and blue arrows in (c) and (d) indicate eastward and westward direction, respectively.

During the 2017 cruise, BLs showed a more coherent distribution from the southern part of the EPFP to the SSS frontal region with BLT maximum occurring in the southern part of the EPFP (~8°N) (Fig. 6a). The distribution of TIs was found in two separate regions within the middle of the EPFP (8.5°−10°N) and in the FTZ (7°−7.5°N) (Fig. 6b). BLs within the EPFP were detected only south of 11°N (Fig. 6a). BLs were thicker than those found during the 2016 cruise with BLT > 50 dbar found in the SSS frontal region. TIs were found mostly concentrated in the EPFP around ~9.5°N and in the FTZ around 7°N (Fig. 6b).

A representative meridional transect along 125°W, which is the longest of the seven transects that sampled across all three regimes during the 2017 cruise, shows ILD increased southward from 30 dbar at 12.5°N in the EPFP to 80 dbar at 6.5°N in the SSS front while MLD was mostly shallower than 50 dbar, resulting in BLs occurring only south of 10°N (Fig. 7a). BLTs exceeded 30 dbar in the FTZ at ~8°N due to a surface puddle of fresher water that resulted in very shallow mixed layers (Figs. 7a and c). TIs were also confined to occur mostly south of 10°N and were associated with a subsurface layer where $\theta > 28.2$°C (Fig. 7b). The strongest TI amplitudes with $\Delta\theta > 0.2$°C were mostly observed in the southern part of the EPFP between 8°−10°N (Fig. 7c).

For all the meridional transects along 125°W during the 2017 cruise, the mean ILD increases southward from 44.46 dbar in the EPFP to 64.08 dbar in the SSS frontal region (Table 1). The mean MLD was shallowest (18.78 dbar) in the FTZ, resulting in the thickest BLs of 39.4 dbar occurring in the FTZ (Table 1). As during the 2016 summer cruise, the frequency of occurrence of BLs was 100% in the FTZ and only 57.5% occurrence in the EPFP (about the same as in 2016) and 79.2% in the SSS front (nearly double as many as found in 2016). Similar to the patterns observed during the 2016 cruise, the mean $\Delta\theta$ in the EPFP (0.19°C) was highest among the three regimes, while TIs were most frequently observed in the FTZ.

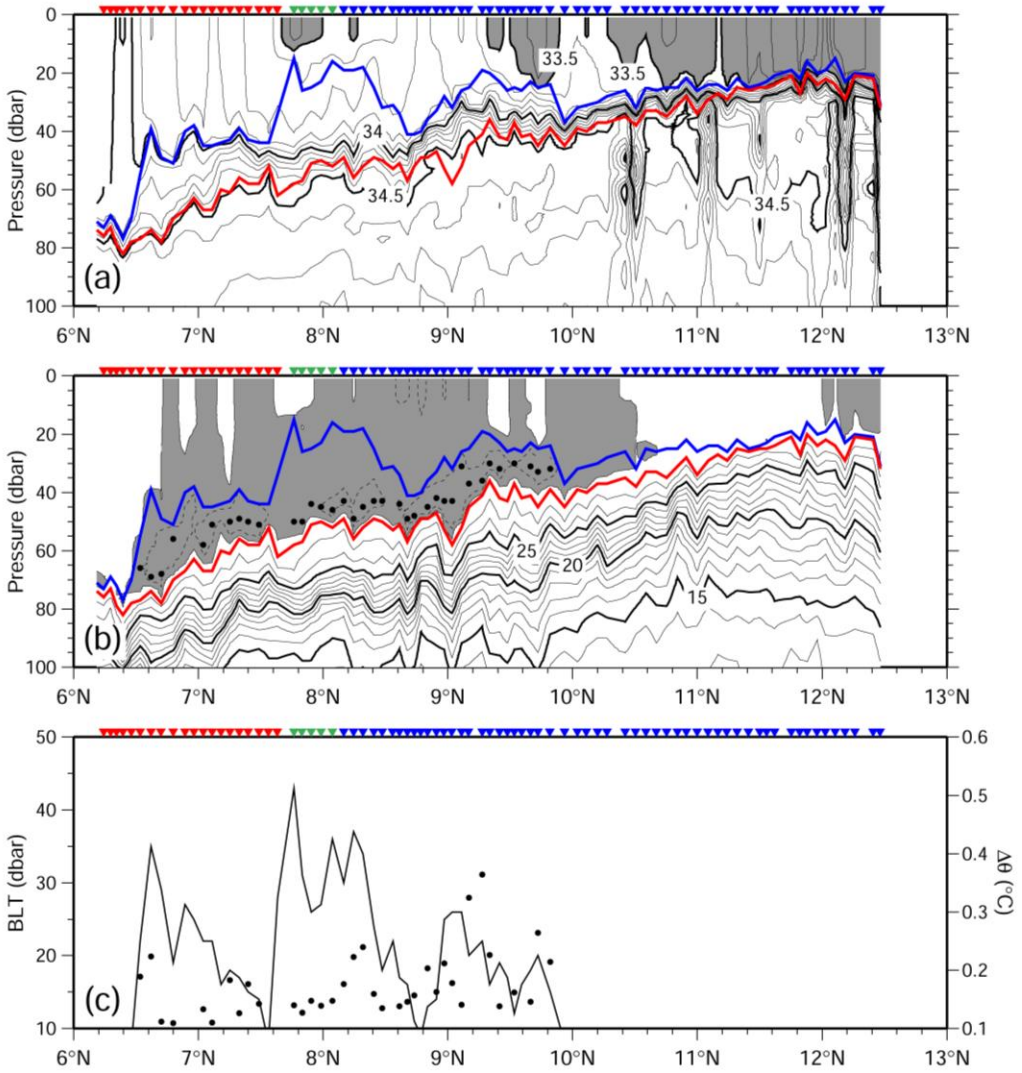

Figure 7. Meridional transects of (a) salinity and (b) θ (°C), and (c) distribution of BLT (dbar; line) and $\Delta\theta$ (°C; dots) along 125°W from uCTD profiles observed during 3−5 November 2017 (red triangles in Figure 2b). Inverted triangles at the top of each panel indicate the locations of uCTD profiles in the EPFP (blue), the FTZ (green), and the SSS front (red). Gray shading in (a) and (b) indicates salinity lower than 33.5 and θ higher than 28°C, respectively, and blue and red curves indicate the MLD and ILD, respectively. Dashed contours in (b) denote θ = 28.2°C. Black dots in (b) denote the depth of the vertical temperature maximum where $\Delta\theta > 0.1$°C.

3.2 Contribution of precipitation and Ekman advection to BL and TI formation

Formation of BLs can be attributed to freshening near the sea surface and/or salinification in the subsurface resulting from different processes (Cronin and McPhaden 2002; Katsura et al. 2015). In the EPFP, on seasonal time scales, Ekman advection works to both freshen and cool the mixed layer in boreal autumn and contributes to BL and TI formation through the tilting of the SSS front (KS2020). Precipitation also contributes to BL formation in the EPFP region in boreal summer. In this subsection, we assess the formation of BL and TI formation through

precipitation and Ekman advection on more synoptic spatio-temporal scales using measurements from the SPURS-2 cruises.

Here, we estimate the contribution of Ekman advection and precipitation to BL formation through surface freshening within the SPURS-2 region, based on uCTD and CTD profiles (Fig. 3). We use the mixed layer salinity budget equation (Ren and Riser, 2009; Katsura et al., 2013) to better understand what processes might result in the BL and TI formation observed during the SPURS-2 cruises. The precipitation term was calculated as

$$S_{prec} = -\frac{PS_m}{h_m}, \quad (1)$$

where P is precipitation, S_m is mixed layer salinity, h_m is MLD. P was obtained from the nearest IMERG grid point to each uCTD and CTD profile and averaged over 24-hours prior to the time of each uCTD and CTD cast. Meridional Ekman salinity and temperature advection terms were calculated as

$$S_{Ek} = -v_{Ek}\frac{\partial S_m}{\partial y} \quad (2)$$

and

$$T_{Ek} = -v_{Ek}\frac{\partial T_m}{\partial y}, \quad (3)$$

respectively, where T_m is mixed layer temperature and v_{Ek} is the meridional Ekman velocity. The meridional differentiation was determined from the uCTD profiles along the 125°W transects during each cruise, as well as the shorter sections along 124°W and 125.5°W in 2017 (Fig. 3). Meridional Ekman velocity v_{Ek} was calculated as

$$v_{Ek} = -\frac{\tau^x}{\rho_0 f h_m} \quad (4)$$

where τ^x is zonal wind stress (positive eastward), ρ_0 is the reference density of seawater, taken to be 1025 kg m^3, and f is the Coriolis parameter. Zonal wind stress τ^x measured during the cruise was averaged over 1-hour prior and posterior to the time of each uCTD and CTD cast (Figs. 4c and 6c). Here, we only focus on freshening and cooling (i.e., negative values of precipitation and Ekman advection terms), which respectively contribute to BL and TI formation.

During the SPURS-2 2016 summer cruise, precipitation and associated surface freshening were largest in the EPFP under the ITCZ but mainly occurred north of the thickest BLs in the SSS front and the FTZ (Figs. 4a, 8a and Table 2).

For all the meridional transects along 125°W, the highest mean values of P (0.240 mm hr^{-1}) and S_{prec} (-0.084 × 10^{-6} s^{-1}) occurred in the EPFP, compared to the FTZ (0.052 mm hr^{-1} and -0.023 × 10^{-6} s^{-1}, respectively) and the SSS frontal region (0.057 mm hr^{-1} and -0.030 × 10^{-6} s^{-1}, respectively) (Table 2). This is in contrast to where the thickest BLs were found in the FTZ and the SSS front (Table 1). In the EPFP and the FTZ, 46.3% and 50.0% of the uCTD profiles were associated with both the presence of a BL and precipitation freshening, respectively. Whereas in the SSS front only 29.3% of casts showed the co-occurrence of both BL and precipitation. The discrepancy between the location of the precipitation maximum and the location of the BLT maximum in boreal summer is consistent with the seasonal climatology of KS2020.

During the SPURS-2 2017 cruise, similar to that found in the 2016 summer cruise, the surface freshening due to precipitation was larger in the EPFP than in both the SSS front and the FTZ (Fig. 8b and Table 2) where the thick BLs were found (Table 1). The precipitation maximum was located between 7.5°−12°N and mean precipitation was larger during this 2017 cruise than during the 2016 boreal summer cruise (Fig. 8b). Freshening due to precipitation associated with the precipitation maximum which exceeded 0.4 mm hr^{-1}, corresponded to where the BLs were thickest in the southern part of the EPFP (Fig. 6a). In contrast, thick BLs in the SSS front and in the FTZ between 6°−7.5°N were located south of the ITCZ and were not associated with freshening due to precipitation.

For all the meridional transects along 125°W during the 2017 cruise, the mean values of P (0.288 mm hr^{-1}) and S_{prec} (-0.108 × 10^{-6} s^{-1}) in the EPFP were largest of the three regimes compared to the FTZ (0.186 mm hr^{-1} and -0.090 × 10^{-6} s^{-1}) and the SSS frontal region (0.139 mm hr^{-1} and -0.034 × 10^{-6} s^{-1}) (Table 2). In the EPFP and the FTZ, nearly half of all the uCTD profiles (51.8% and 50.0%, respectively) were associated with both BL and precipitation freshening, while only 18.9% of profiles showed concurrent BL presence and precipitation in the SSS front.

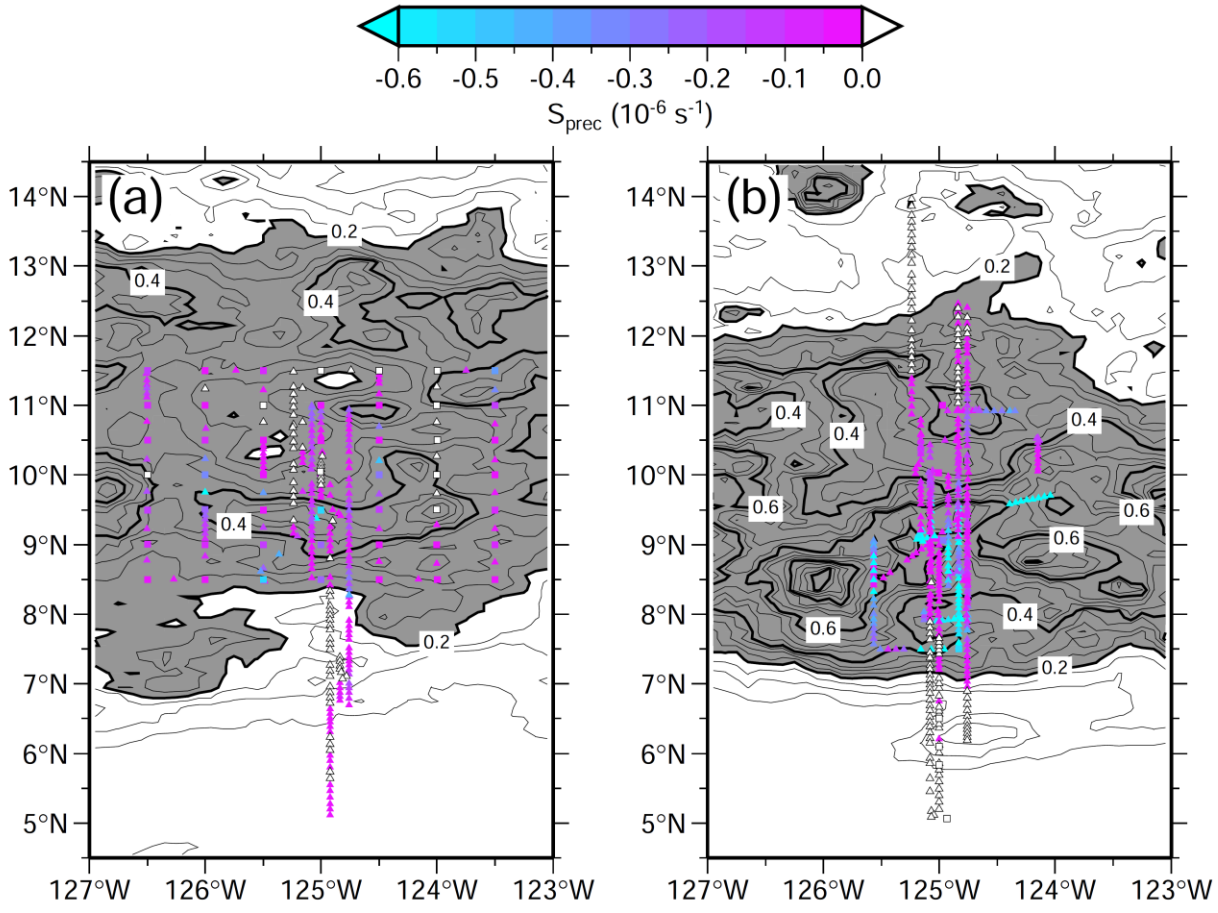

Figure 8. Distribution of S_{prec} from uCTD (colored triangles and circles) and CTD (colored squares) profiles during the SPURS-2 (a) 2016 cruise and (b) 2017 cruise. Triangles along 125°W are slightly shifted zonally to improve visibility. Note only freshening (S_{prec} < 0) is shown by the negative color bar. White symbols indicate the value of zero. Contours indicate

405 the mean precipitation from IMERG (mm hour^{-1}) (a) from 21 August to 12 September 2016 and
406 (b) from 21 October to 11 November 2017. Gray shading indicates precipitation higher than 0.2
407 mm hour^{-1}.

		P (mm hour^{-1})	S_{prec} (10^{-6} s^{-1})	Number of Profile with BL and $S_{prec} < 0$ and Frequency
2016	EPFP	0.240 (0.041)	-0.084 (0.016)	62 (46.3%)
	FTZ	0.052 (0.013)	-0.023 (0.012)	7 (50.0%)
	SSS front	0.057 (0.033)	-0.030 (0.018)	12 (29.3%)
2017	EPFP	0.288 (0.091)	-0.108 (0.039)	117 (51.8%)
	FTZ	0.186 (0.140)	-0.090 (0.080)	9 (50.0%)
	SSS front	0.139 (0.113)	-0.034 (0.029)	10 (18.9%)

408

409 Table 2. Mean values of P and S_{prec} and the number of profiles with both $S_{prec} < 0$ and a BL in
410 the EPFP, the FTZ, and the SSS front along the 125°W transects during the 2016 and 2017
411 cruises. Values in parentheses indicate the 95% confidence interval. Calculation of mean P and
412 mean S_{prec} was performed only for uCTD profiles with $S_{prec} < 0$. Frequency of profiles with both
413 BLT > 10 dbar and $S_{prec} < 0$ were relative to the total number of profiles in each regime.

414 During the 2016 boreal summer cruise, Ekman advection of fresher and cooler water
415 contributed to BL and TI formation in both the EPFP and in the SSS front (Fig. 9, Table 3).
416 Freshening due to Ekman advection occurred north of 9°N in the EPFP (Fig. 9a). Ekman
417 advection also worked to cool the mixed layer north of 9°N in the high SST region (Fig. 9b).
418 The southward Ekman advection in the EPFP resulted from the northeastward wind, while the
419 northward Ekman flow in the SSS front resulted from northwestward wind (Table 2, Fig. 4c).

420 The mean Ekman advection from all the 2016 125°W transects shows that freshening in
421 the EPFP (-0.202×10^{-6} s^{-1}) was larger than in the SSS front (-0.130×10^{-6} s^{-1}), while mean
422 Ekman cooling in the SSS front (-0.358×10^{-6} °C s^{-1}) was double that in the EPFP (-0.166×10^{-6} °C s^{-1}) (Table 2). In the FTZ, the weak meridional Ekman velocity beneath the ITCZ led to the
424 weakest Ekman freshening (-0.064×10^{-6} s^{-1}) and cooling (-0.039×10^{-6} °C s^{-1}) among the three
425 regimes. However, the frequency of coincidence of both BL and Ekman freshening (TI and
426 Ekman cooling) was 31.3% (20.6%) in the EPFP and only 20.5% (2.6%) in the SSS frontal
427 region, much less than the 61.5% (30.8%) occurrence in the FTZ (Table 3). Overall, for the
428 three regimes, the freshening and cooling by Ekman advection showed a patchy and/or porous
429 distribution (Fig. 9), with 31.1% (17.5%) of all profiles associated with both BL and Ekman
430 freshening (TI and Ekman cooling).

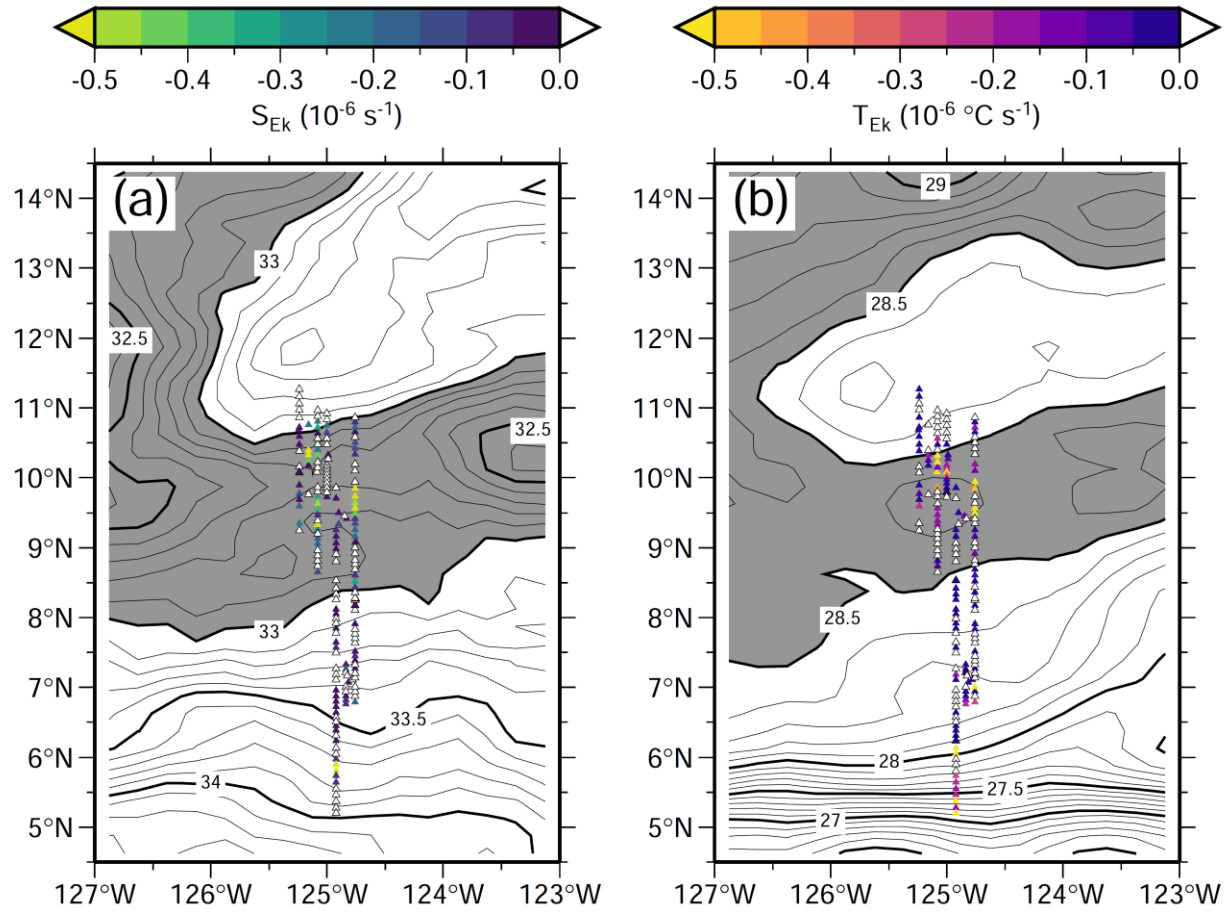

Figure 9. Distribution of (a) S_{Ek} and (b) T_{Ek} from uCTD profiles along 125°W during the SPURS-2 2016 cruise (colored triangles). Triangles along 125°W are slightly shifted zonally to improve visibility. Note only freshening ($S_{Ek} < 0$) and cooling ($T_{Ek} < 0$) are shown, as indicated by the negative color bars. White triangles indicate positive values (salinification and warming). Contours indicate (a) the mean SSS from SMAP and (b) the mean SST from OISST (°C) from 21 August to 12 September 2016. Gray shading indicates (a) SSS lower than 33.0 and (b) SST higher than 28.5°C.

		v_{Ek} (m s^{-1})	S_{Ek} (10^{-6} s^{-1})	T_{Ek} (10^{-6} °C s^{-1})	Number of Profiles with BL and $S_{Ek} < 0$ and Frequency	Number of Profiles with TI and $T_{Ek} < 0$ and Frequency
2016	EPFP	-0.024 (0.007)	-0.202 (0.061)	-0.166 (0.066)	41 (31.3%)	27 (20.6%)
	FTZ	0.003 (0.010)	-0.064 (0.049)	-0.039 (0.022)	8 (61.5%)	4 (30.8%)
	SSS front	0.037 (0.011)	-0.130 (0.113)	-0.358 (0.248)	8 (20.5%)	1 (2.6%)
2017	EPFP	0.013 (0.006)	-0.141 (0.039)	-0.090 (0.023)	67 (29.9%)	36 (16.1%)
	FTZ	0.006 (0.031)	-0.169 (0.167)	-0.220 (0.096)	8 (44.4%)	8 (44.4%)
	SSS front	0.010 (0.026)	-0.314 (0.172)	-0.236 (0.102)	17 (32.7%)	6 (11.5%)

Table 3. Mean values of v_{Ek}, S_{Ek} and T_{Ek} and the number of profiles with both a BL and $S_{Ek} < 0$ and a TI and $T_{Ek} < 0$ in the EPFP, the FTZ, and the SSS front along the 125°W transects during the 2016 and 2017 cruises. Values in the parentheses indicates the 95% confidence interval.

Calculation of mean S_{Ek} and mean T_{Ek} was performed only for uCTD profiles with $S_{Ek} < 0$ and $T_{Ek} < 0$, respectively. Frequency of profiles was relative to the total number of profiles in each regime.

During the 2017 boreal autumn cruise, both freshening and cooling by Ekman advection were found in the three regimes, but were maximum in the SSS front (Fig. 10 and Table 3), coinciding with where thick BLs with TIs were found (Figs. 6a and b). North of about 8.5°N in the EPFP, the magnitude of both Ekman freshening and cooling was much smaller. In general, both Ekman freshening and cooling showed a patchy and porous distribution (Fig. 10).

For all the meridional transects along 125°W during the boreal autumn, the mean amplitude of Ekman freshening and cooling was weakest in the EPFP (-0.141×10^{-6} s^{-1} and -0.090×10^{-6} °C s^{-1}, respectively), increasing southward to the SSS frontal region (-0.314×10^{-6} s^{-1} and -0.236×10^{-6} °C s^{-1}, respectively) (Table 3). The coincidence of both Ekman freshening and BL presence in the FTZ was 44.4%, but only 29.9% in the EPFP and 32.7% in the SSS front. The coincidence of both Ekman cooling and TIs occurred mostly in the FTZ (44.4%), compared to the EPFP (16.1%) and the SSS frontal region (11.5%). As in the 2016 summer cruise, the coincidence of Ekman advection with BLs and TIs was found in less than half of all profiles where BLs and TI occurred (Table 2), again suggesting a patchy distribution of Ekman freshening and cooling. Overall, for the three regimes, the coincidence of both BLs and Ekman freshening (TIs and Ekman cooling) was found in 34.6% (14.7%) of all profiles.

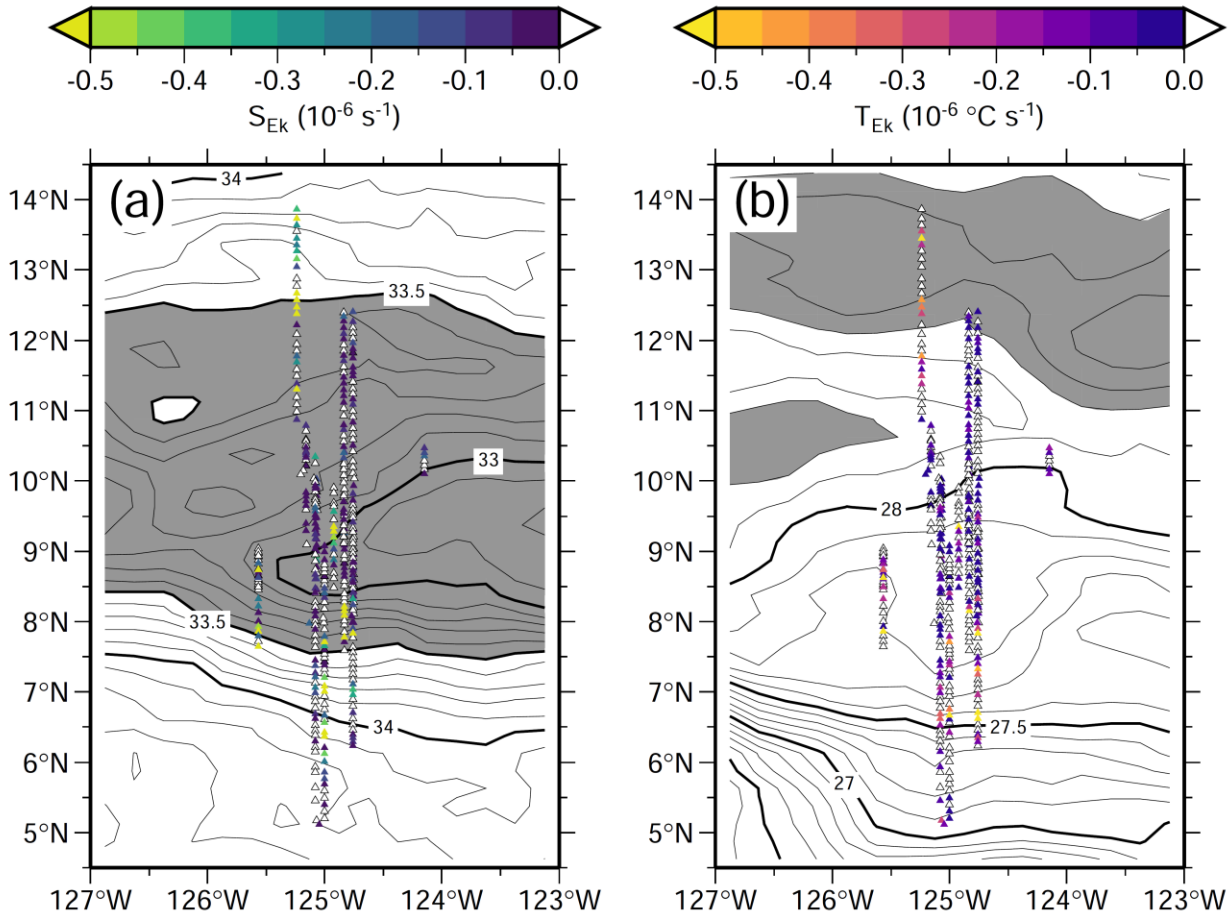

Figure 10. Distribution of (a) S_{Ek} and (b) T_{Ek} from uCTD profiles during the SPURS-2 2017 cruise (triangles). Triangles along 125°W are slightly shifted zonally to improve visibility. Note only freshening ($S_{Ek} < 0$) and cooling ($T_{Ek} < 0$) are shown, as indicated by the negative color bars. White triangles indicate positive values (salinification and warming). Contours indicate (a) the mean SSS from SMAP and (b) the mean SST from OISST (°C) from 21 October to 11 November 2017. Gray shading indicates (a) SSS lower than 33.5 and (b) SST higher than 28.2°C.

3.3 BL and TI Formation through the Tilting Process

Ekman advection worked to freshen and cool the mixed layer both in the EPFP and in the SSS front during the 2016 cruise and in the SSS frontal region during the 2017 cruise. To test whether this Ekman advection resulted in formation of BLs with TIs through the tilting of the SSS front, the rate of net change of salinity ($S_{tilting}$; s^{-1}) and temperature ($T_{tilting}$; °C s^{-1}) in the surface layer caused by the vertically sheared meridional velocity to the vertical salinity and temperature gradient within the isothermal layer was calculated as

$$S_{tilting} = -\left(v_{surface} - v_{ILD}\right)\frac{\partial S_m}{\partial y} \quad (5)$$

and

$$T_{tilting} = -\left(v_{surface} - v_{ILD}\right)\frac{\partial T_m}{\partial y}, \quad (6)$$

where $v_{surface}$ and v_{ILD} are meridional velocity at the sea surface and at the ILD, respectively (Cronin and McPhaden 2002). Negative $S_{tilting}$ ($T_{tilting}$) indicates a net freshening (cooling) at the sea surface caused by the tilting process. Surface meridional velocity $v_{surface}$ was derived from the shallowest bin of the ADCP velocity (typically ~17 dbar) while v_{ILD} was velocity at the depth of the ILD. When the ILD was shallower than the shallowest bin of the ADCP velocity, the calculation of $S_{tilting}$ and $T_{tilting}$ was not defined. Among the uCTD profiles used for the calculation of the advection term, only 15 (8.2%) and 1 (0.2%) uCTD profiles had ILD < 17 dbar for the 2016 and 2017 cruises, respectively, and so were omitted from the calculation. Finally, both $v_{surface}$ and v_{ILD} were averaged over 1-hour prior and posterior to the time of each uCTD cast (Figs. 4d and 6d).

During the 2016 cruise, the tilting process was found to contribute to BL and TI formation both in the EPFP and in the SSS frontal region, with the largest contribution in the FTZ (Fig. 11 and Table 4). In the EPFP, freshening and cooling by the tilting process was found between 9.5°−11°N and also at ~7°N (Figs. 11a and b). These regions correspond to the distribution of thick BLs with TIs (Figs. 4a and b), consistent with BL and TI formation through the tilting process in KS2020.

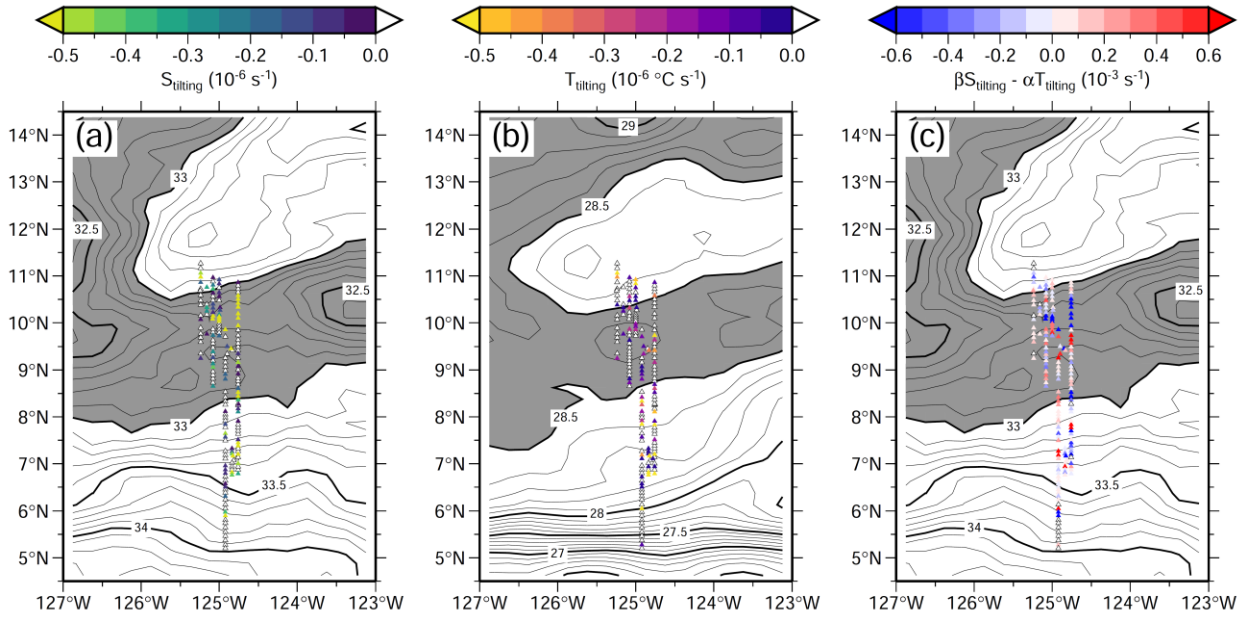

Figure 11. Distribution of (a) $S_{tilting}$, (b) $T_{tilting}$, and (c) $\beta S_{tilting}$ - $\alpha T_{tilting}$ from uCTD profiles along 125°W during the SPURS-2 2016 cruise (colored triangles). Triangles along 125°W are slightly shifted zonally to improve visibility. Note only freshening ($S_{tilting} < 0$) and cooling ($T_{tilting} < 0$) are shown in (a) and (b), respectively, as indicated by the negative color bars. White triangles indicate positive values (salinification and warming) or undefined values. Contours indicate (a and c) the mean SSS from SMAP and (b) the mean SST from OISST (°C) from 21 August to 12 September 2016. Gray shading indicates (a and c) SSS lower than 33.0 and (b) SST higher than 28.5°C.

For all the meridional transects along 125°W during 2016, mean freshening (-0.644×10^{-6} °C s^{-1}) and cooling (-0.762×10^{-6} °C s^{-1}) caused by tilting were largest in the FTZ among the three regimes (Table 4). However, the Ekman contribution to freshening and cooling was found to be very weak in the FTZ (Table 3), implying that geostrophic advection mainly contributes to the tilting process in the FTZ. The frequency of BL occurrence associated with tilting and freshening was 61.5% in the FTZ but only 31.2% in the EPFP and 26.7% in the SSS front. The frequency of TI occurrence associated with tilting and cooling was also higher in the FTZ (30.8%) compared to the EPFP (16.0%) and the SSS front (3.3%). These results indicate that the FTZ is a critical region for BL and TI formation through tilting due to geostrophic advection. Overall, for the three regimes, the freshening and cooling showed a patchy and porous distribution in the SPURS-2 region (Figs. 11a and b) with only 30.1% (13.7%) of all profiles associated with concurrence of both BL (TI) and freshening (cooling) due to the tilting process.

		$S_{tilting}$ (10^{-6} s^{-1})	$T_{tilting}$ (10^{-6} °C s^{-1})	Number of Profile with BL and $S_{tilting} < 0$ and Frequency	Number of Profile with TI and $T_{tilting} < 0$ and Frequency	Number of Profile with BL and $-1 < R_y < 1$ and Frequency	Number of Profile with TI and $0 < R_y < 1$ and Frequency
2016	EPFP	-0.472 (0.146)	-0.245 (0.079)	39 (31.2%)	20 (16.0%)	66 (50.8%)	14 (10.8%)
	FTZ	-0.644 (0.677)	-0.762 (1.196)	8 (61.5%)	4 (30.8%)	9 (69.2%)	5 (38.5%)
	SSS front	-0.526 (0.320)	-0.555 (0.500)	8 (26.7%)	1 (3.3%)	14 (35.9%)	0 (0%)
2017	EPFP	-0.441 (0.102)	-0.285 (0.066)	66 (29.6%)	38 (17.0%)	102 (45.7%)	35 (15.7%)
	FTZ	-0.394 (0.425)	-0.992 (0.527)	8 (44.4%)	7 (38.9%)	11 (61.1%)	6 (33.3%)
	SSS front	-0.161 (0.148)	-0.338 (0.150)	11 (21.2%)	8 (15.4%)	32 (61.5%)	4 (7.7%)

Table 4. Mean values of $S_{tilting}$ and $T_{tilting}$ and the number of profiles with both BL and where $S_{tilting} < 0$ and $-1 < R_y < 1$; and the number of profiles with both TI and where $T_{tilting} < 0$ and $0 < R_y < 1$ in the EPFP, the FTZ, and the SSS front along the 125°W transects during the 2016 and 2017 cruises. Values in the parentheses indicates the 95% confidence interval. Calculation of mean $S_{tilting}$ and mean $T_{tilting}$ was performed only for uCTD profiles with $S_{tilting} < 0$ and $T_{tilting} < 0$, respectively. Frequency of profiles was relative to the total number of profiles in each regime.

During the 2017 cruise, the contribution of tilting to BL and TI formation was found broadly spread over in the SPURS-2 region, indicating patchiness and porosity (Fig. 12). Freshening and cooling by tilting were strongest in the EPFP and the FTZ, respectively (Table 4). Freshening due to tilting was broadly spread occurring mainly from the FTZ at ~7°N to the middle of the EPFP at ~10.5°N (Fig. 12a) where thick BLs were also found (Fig. 6a). The tilting also resulted in cooling between 6.5°−8°N in the SSS front and the FTZ and between 8.5°−10°N in the EPFP (Fig. 12b). These latitudes corresponded to the location of the warmest TIs (Fig. 6b).

For all 125°W meridional transects during 2017, freshening by tilting in the EPFP (-0.441 × 10^{-6} s^{-1}) and the FTZ (-0.394 × 10^{-6} s^{-1}) were more than twice as strong as found in the SSS front (-0.161 × 10^{-6} s^{-1}; Table 4). Cooling by tilting was strongest in the FTZ with a mean value of -0.992 × 10^{-6} °C s^{-1}. The meridional difference in the tilting process between the three regimes is opposite to that found for Ekman advection, which is highest within the SSS front (Table 3). The frequency of BL occurrence associated with both tilting and freshening was highest in the FTZ (44.4%) compared to the EPFP (29.6%) and the SSS front (21.2%). The frequency of TI occurrence in profiles associated with tilting and cooling was also highest in the FTZ (38.9%) compared to the EPFP (17.0%) and the SSS front (15.4%). As in the 2016 cruise, these results confirm that the FTZ is a critical region for BL and TI formation through the tilting process and that the geostrophic component is dominant. Overall, for the three regimes, the coincidence of tilting and freshening with BL presence was found in 34.6% of all profiles, and the coincidence of tilting and cooling with TI presence was found in 16.5% of all profiles.

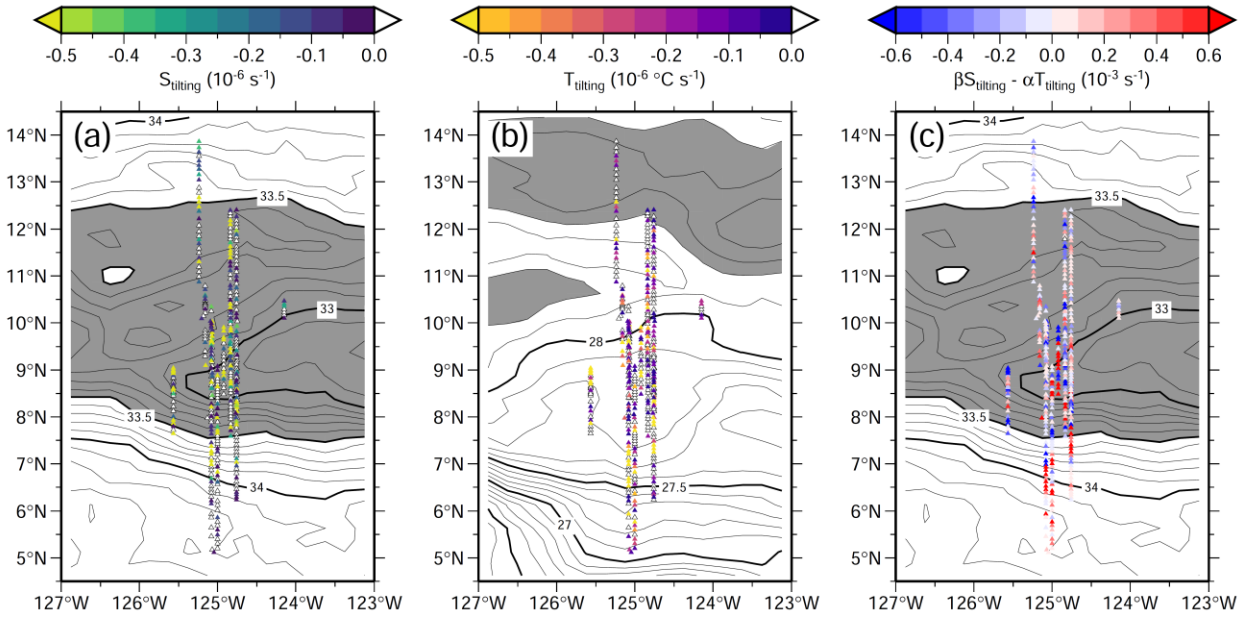

Figure 12. Distribution of (a) $S_{tilting}$, (b) $T_{tilting}$, and (c) $\beta S_{tilting}$ - $\alpha T_{tilting}$ from uCTD profiles during the SPURS-2 2017 cruise (triangles). Triangles along 125°W are slightly shifted zonally for improved visibility. White triangles indicate undefined values. Note only freshening ($S_{tilting} < 0$) and cooling ($T_{tilting} < 0$) are shown in (a) and (b), respectively, as indicated by the negative color bars. White triangles indicate positive values (salinification and warming) or undefined values. Contours indicate (a and c) the mean SSS from SMAP and (b) the mean SST from OISST (°C) from 21 October to 11 November 2017. Gray shading indicates (a and c) SSS lower than 33.5 and (b) SST higher than 28.2°C.

Net strong freshening and cooling at the sea surface was caused by tilting of isohalines and isotherms in the SPURS-2 region, particularly in the FTZ, which are favorable to the formation of BLs with TIs. To further explore the possibility of BL and TI formation through tilting, the meridional density ratio R_y (Tippins and Tomczak 2003; Katsura et al. 2015) was calculated as

$$R_y = \frac{\alpha\, \partial T/\partial y}{\beta\, \partial S/\partial y} \tag{7}$$

where α is the thermal expansion coefficient and β is the saline contraction coefficient. Here we use SST from OISST and SSS from SMAP as well as near-surface temperature and salinity values from uCTD profiles during the cruise periods. For BL formation through the tilting process, the contribution of the salinity gradient to the density gradient must be larger than that of the temperature gradient in the horizontal direction in order to maintain vertical stability after BL formation, and so $-1 < R_y < 1$ must be satisfied (Katsura et al., 2015). For TI formation, the horizontal salinity and temperature gradient must have a compensating contribution to the horizontal density gradient, meaning that $0 < R_y < 1$ must be satisfied (KS2020). These R_y conditions for BL ($-1 < R_y < 1$) and TI ($0 < R_y < 1$) formation are due to the need for stability in the MLDs associated with BLs and TIs (Mignot et al., 2012).

During the 2016 cruise, the condition for BL formation was satisfied over the most of the SPURS-2 region, and the condition for TI formation was satisfied in the southern part of the EPFP and the FTZ (Fig. 13). In general, R_y in the EPFP was mostly positive in the southern part of the EPFP (Fig. 13a), as well as in the mixed layer along 125°W (Fig. 13b), corresponding to where BLs with TIs occurred (Figs. 4a and b). Although R_y was mostly negative south of 8°N in the mean state during the 2016 cruise (Fig. 13a), positive R_y was found in the uCTD profiles at ~ 7°N in the FTZ. This distribution of R_y corresponded to the region with thick BLs and TIs (Figs, 4b and 13b), confirming their formation through the tilting process. Indeed, the distribution of $\beta S_{tilting}$ - $\alpha T_{tilting}$, which is the net density change due to tilting, was significantly correlated (R = 0.94) with $S_{tilting}$ (Figs. 11a and c) during the 2016 summer cruise, indicating that it is the freshening due to tilting that leads to a net decrease of surface density and hence BL formation. In contrast, the net density change from temperature had a -0.53 correlation. This negative correlation indicates that the net decrease of surface density caused by the tilting due to freshening (i.e. where $\beta S_{tilting}$ - $\alpha T_{tilting} < 0$) tends to be associated with where the conditions are unfavorable to TI formation through cooling (i.e., where $R_y < 0$). Similar to the tilting components (Fig. 11), R_y also showed a patchy distribution (Fig. 13b) and the coincidence of BL (TI) with where $-1 < R_y < 1$ ($0 < R_y < 1$) occurred in 48.9% (10.4%) of all uCTD profiles during the cruise.

For all the meridional transects along 125°W during summer 2016, the frequency of BL occurrence with $-1 < R_y < 1$ was highest in the FTZ (69.2%), compared to the EPFP (50.8%) and

591 the SSS front (35.9%) (Table 4). This is consistent with the highest frequency of BL occurring
592 where there is freshening due to tilting in the FTZ (Table 4). The frequency of TI occurring with
593 where $0 < R_y < 1$ was also highest in the FTZ (38.5%) compared to the EPFP (10.8%) and the
594 SSS front (0%). This agrees with the finding that most TIs occur where there is cooling due to
595 the tilting process in the FTZ. This is also consistent with BL and TI formation occurring
596 through the tilting process, especially in the FTZ.

597 During the 2017 cruise, the $-1 < R_y < 1$ required for BL formation was broadly satisfied in
598 the SPURS-2 region (Fig. 14a). Positive R_y was generally found in the EPFP between
599 8.5°−13°N in both the mean SSS and SST (Fig. 14a) and the uCTD profiles along 125°W (Fig.
600 14b). Although R_y derived from mean SSS and SST was negative in the SSS front (Fig. 14a),
601 positive R_y was detected in the uCTD profiles in the FTZ at ~7°N where TIs occurred (Figs. 6b
602 and 14b). This correspondence of R_y to the presence of BLs and TIs further confirms the
603 formation of BLs and TIs through the tilting process. As in the 2016 cruise, the distribution of
604 $\beta S_{tilting} - \alpha T_{tilting}$ was highly correlated ($R = 0.96$) with $S_{tilting}$ (Figs. 12a and c), indicating that
605 freshening through tilting works to decrease the surface density and leads to BL formation. The
606 net density change due to the temperature term was again weak, although during the 2017 fall
607 cruise, unlike the 2016 cruise it was positively correlated ($R = 0.27$). This weakly positive
608 correlation indicates that the net decrease of surface density from tilting due to freshening (i.e.
609 where $\beta S_{tilting} - \alpha T_{tilting} < 0$) tends to be associated with where there is cooling, which is favorable
610 to TI formation (i.e., $0 < R_y < 1$). As during the 2016 cruise, R_y also showed a patchy distribution
611 (Fig. 14), with 49.5% (15.4%) of all profiles associated with the presence of a BL (TI) where -1
612 $< R_y < 1$ ($0 < R_y < 1$).

613 For all the meridional transects along 125°W during the 2017 autumn cruise, the frequency
614 of occurrence of BL with where $-1 < R_y < 1$ was higher in both the FTZ (61.1%) and the SSS
615 frontal region (61.5%) than in the EPFP (45.7%) (Table 4). This result is consistent with BL
616 formation through the tilting of isohalines in the FTZ. The frequency of TI occurring with where
617 $0 < R_y < 1$ in the FTZ (33.3%) was higher than in the EPFP (15.7%) and the SSS front (7.7%).
618 Similar to the 2016 cruise, these results show a high occurrence of TI and cooling, and BL and
619 freshening, due to tilting processes in the FTZ (Table 4).

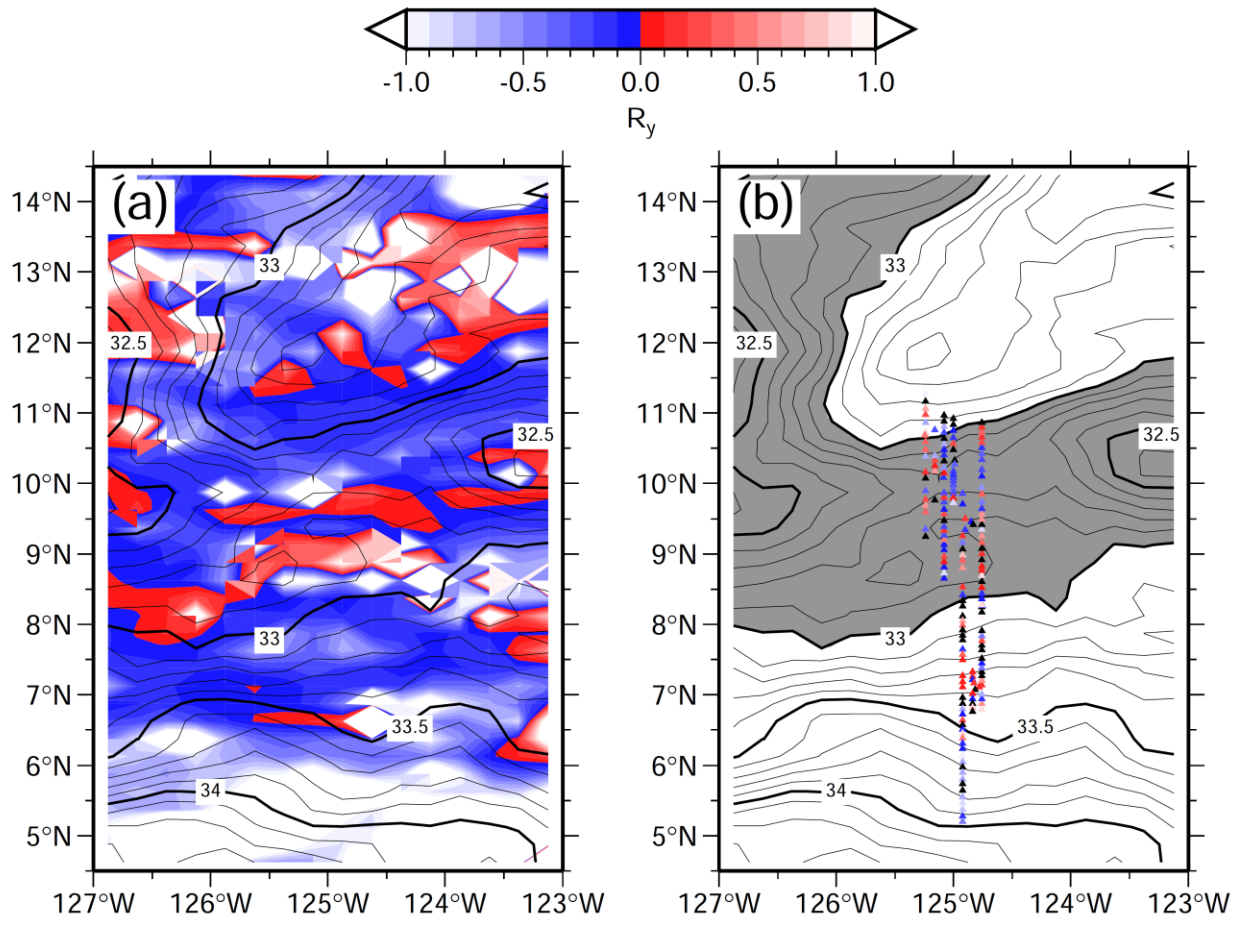

Figure 13. Distribution of R_y at the sea surface (a) based on the mean SSS from SMAP and SST from OISST from 21 August to 12 September 2016 (color) and (b) near-surface temperature and salinity from uCTD measurement along 125°W during the SPURS-2 2016 cruise (triangles). Only values that satisfy the criteria for BL formation ($-1 < R_y < 1$) are shown, as indicated by the color bar. Black triangles are values that are outside the criteria range. Triangles along 125°W in are slightly shifted zonally to improve visibility. Contours indicate the mean SSS from SMAP from 21 August to 12 September 2016. Gray shading in (b) indicates SSS lower than 33.0.

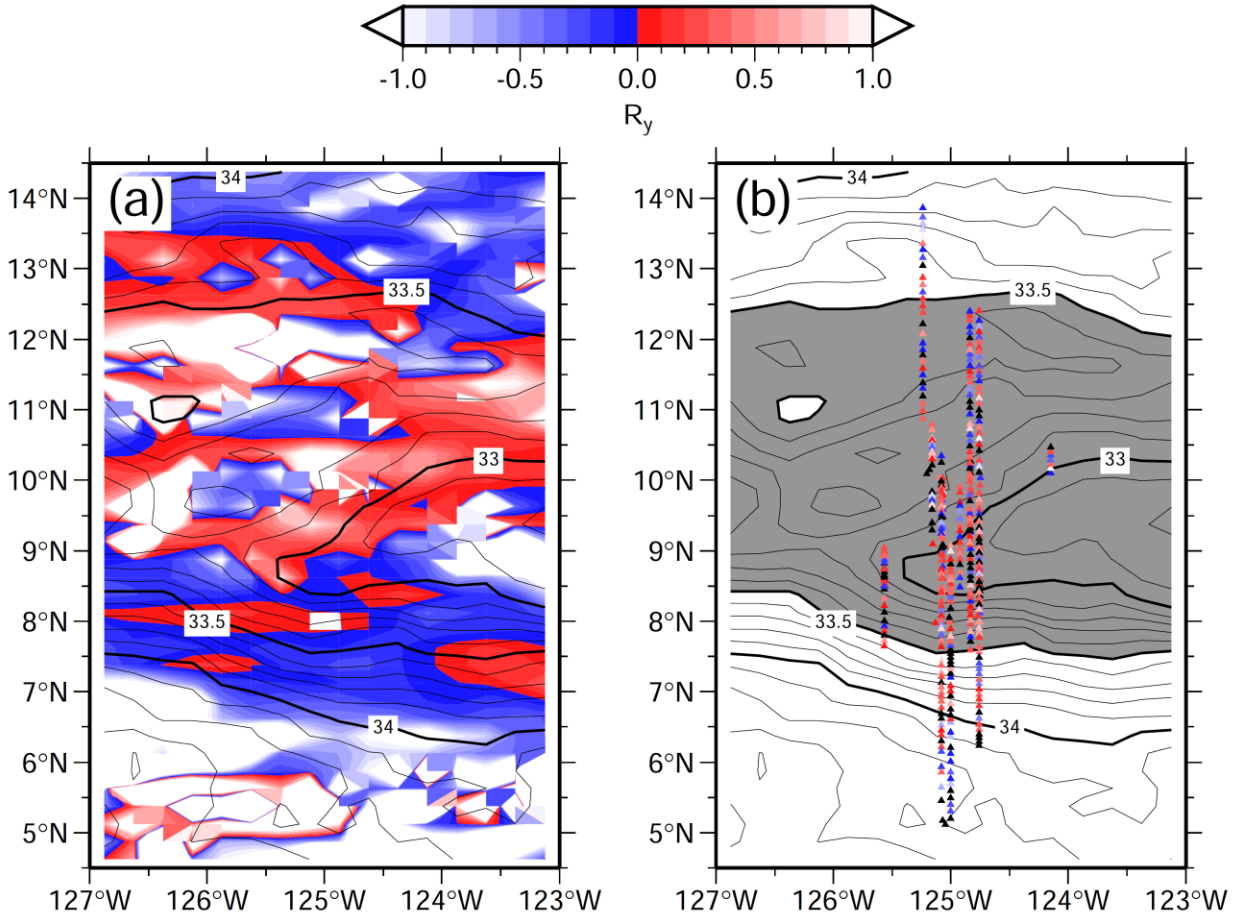

Figure 14. Distribution of R_y at the sea surface (a) based on the mean SSS from SMAP and SST from OISST from 21 October to 11 November 2017 (color) and (b) near-surface temperature and salinity from uCTD measurement during the SPURS-2 2017 cruise (triangles). Only values that satisfy the criteria for BL formation ($-1 < R_y < 1$) are shown, as indicated by the color bar. Black triangles are values that are outside the criteria range. Triangles along 125°W are slightly shifted zonally to improve visibility. Contours indicate the mean SSS from SMAP from 21 October to 11 November 2017. Gray shading in (b) indicates SSS lower than 33.5.

Oxygen profiles from the CTD-O_2 casts enable a unique opportunity to further corroborate whether the cooling and freshening through the tilting process was caused by surface or subsurface flow. If BLs are formed by subsurface processes such as subduction or advection of the higher salinity water within the BL, then dissolved oxygen (DO) should be lower within the BL than within the overlying surface mixed layer due to the oxygen consumption by biological activity. Conversely, if BLs are formed through surface processes such as precipitation and surface advection of fresher water that produce caps of low salinity water in the near-surface, the DO within the BL should be the same or higher than found within the surface mixed layer. Indeed, the DO concentration within BLs in the CTD-O_2 profiles showed almost the same or higher levels compared to levels within the overlying mixed layers (Fig. 15). Here, we defined the MLD_{O2} as the depth at which DO saturation decreases by 1% from the value at 10-dbar, which can be interpreted as a measure of the extent of vertical mixing. Almost all CTD- O_2 profiles during the SPURS-2 cruises showed MLD_{O2} to be deeper than or similar to the

ILD (Figs. 15 and 16). This implies that BLs were formed by surface capping of fresher water induced through surface processes. Indeed, some BLs with TIs contained higher DO water than the overlying mixed layer (Fig. 15). The depth of the vertical oxygen maximum detected in 20 CTD-O_2 profiles during the two SPURS-2 cruises corresponded to the depth of the temperature maximum associated with TIs, with a significant positive correlation (R = 0.87). The subsurface oxygen maximum is known to be prominent during the late summer (Reid, 1962; Jenkins and Goldman, 1985; Hayward, 1994; Sukigara et al., 2011). The subsurface oxygen maximum results from the seasonal pycnocline which prevents photosynthetically-produced oxygen from escaping to the atmosphere (Najjar and Keeling, 1997). Thus, the correspondence of the subsurface temperature and oxygen maxima implies that BLs and TIs were formed through surface processes and confirms that the surface flow plays an important role in the tilting process.

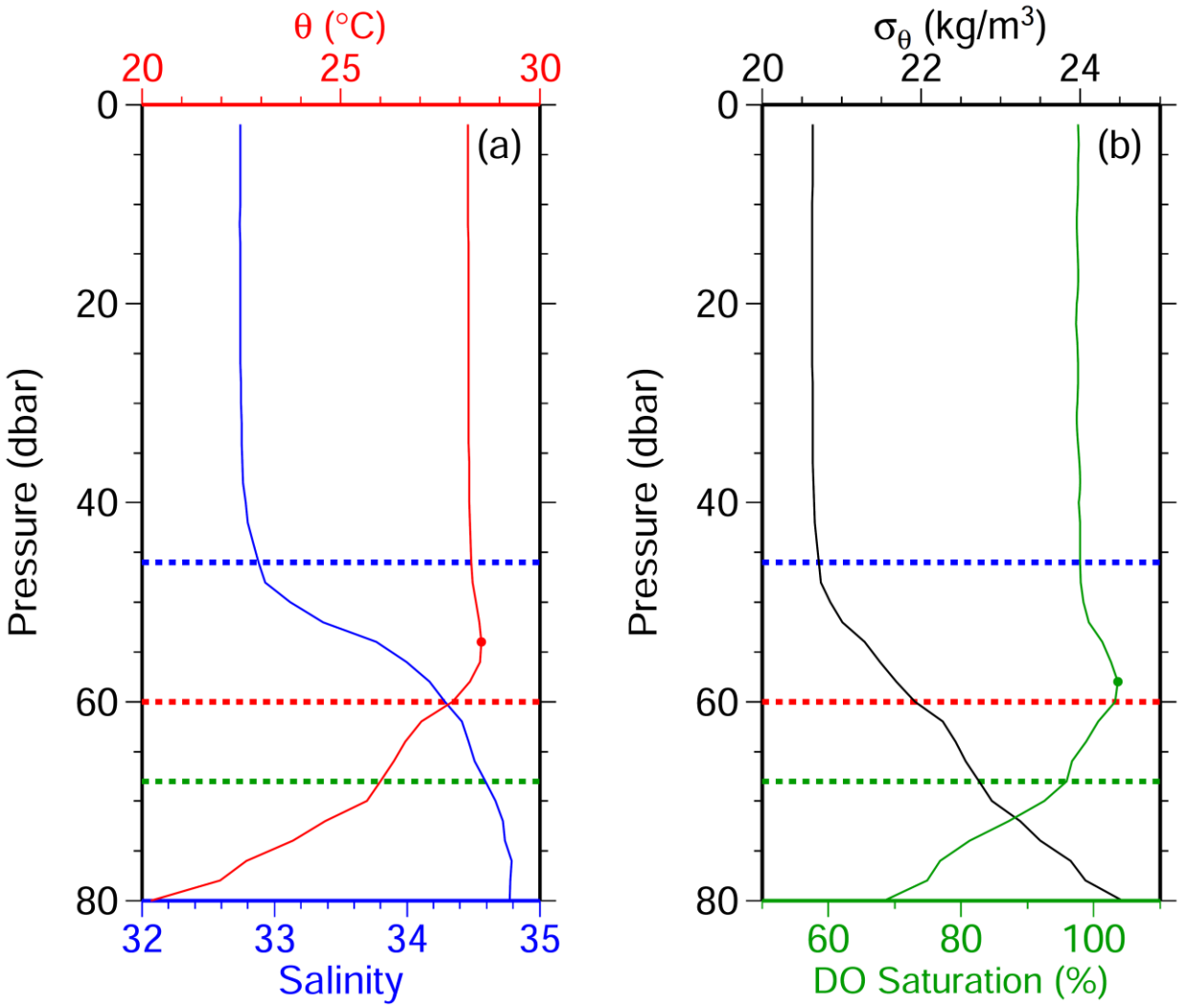

Figure 15. Vertical CTD profile of (a) θ (red curve), salinity (blue curve), (b) σ_θ (black curve), and dissolved oxygen saturation (green curve) at 8.5°N, 124.5°W observed on 4 September 2016. Horizontal red, blue, and green dashed lines indicate the MLD, ILD, and MLD_{O2}, respectively. Red and green dots indicate the vertical temperature and oxygen maximum, respectively.

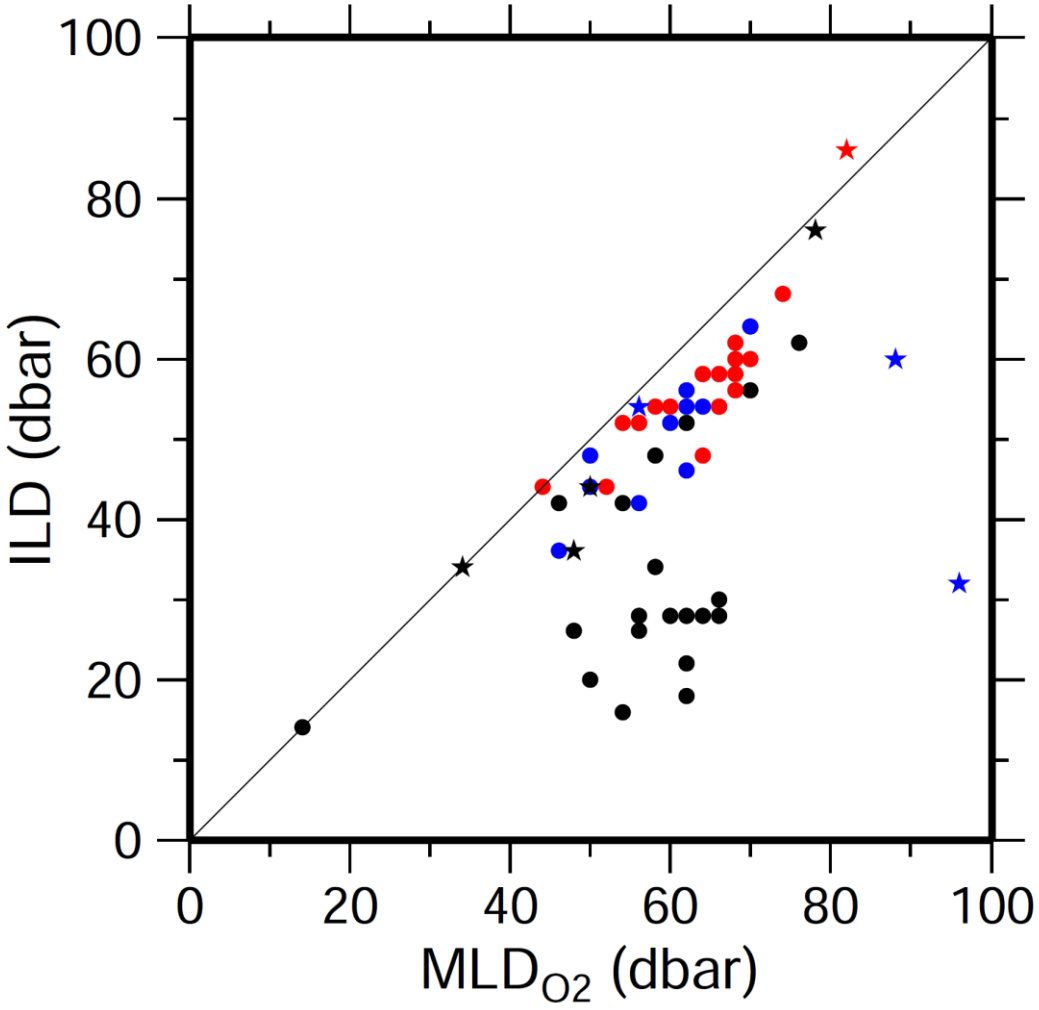

Figure 16. Scatter diagram of the ILD and the MLD_{O2} from CTD-O_2 profiles in the SPURS-2 2016 (circles) and 2017 cruises (stars). Black symbols are for BLT < 10 dbar. Blue symbols are for BLT > 10dbar and $\Delta\theta$ < 0.1℃. Red symbols are for BLT > 10dbar and $\Delta\theta$ > 0.1℃.

4 Discussion and Summary

BLs and associated TIs were investigated, and their formation mechanisms explored using shipboard observations with high spatial resolution during the SPURS-2 cruises. During the 2016 summer cruise, BLs and TIs occurred within the low SSS and high SST region, that corresponded to the EPFP. Thick BLs and warm TIs were also found in the FTZ and the SSS front to the south of the EPFP. During the 2017 autumn cruise, BLs were found in the southern part of the EPFP. BLs in 2017 were thicker than those in 2016, and the thickest BLs were found in the FTZ. In 2017, TIs were also found in the southern part of the SSS front and concentrated in the middle of the EPFP and in the FTZ. During both the 2016 and 2017 cruise, the occurrence of BLs and TIs was most frequent in the FTZ, indicating that the FTZ is the critical region of BL and TI formation.

To investigate the formation mechanisms of BLs and TIs during the SPURS-2 cruises, the contribution of precipitation and meridional Ekman advection to surface freshening were

evaluated. During both cruises, BLs within the EPFP were distributed in the fresher region associated with precipitation under the ITCZ while thick BLs in the SSS front and in the FTZ occurred south of the precipitation maximum. Ekman advection worked to freshen and cool the surface layer in the EPFP and the SSS front, which is favorable to BL and TI formation through the tilting process. During the 2016 cruise, freshening and cooling by Ekman advection were strongest in the EPFP and the SSS front and weak in the FTZ. During the 2017 cruise, freshening and cooling caused by Ekman advection occurred mostly in the SSS front compared to the EPFP and the FTZ.

To further assess the formation of BLs and TIs through tilting, the net surface freshening and cooling due to the vertically sheared velocity within the isothermal layer was examined. During the 2016 and 2017 cruises, tilting processes contributed to both freshening and cooling from the SSS front to the EPFP and corresponded to the prevalence of BLs and TIs. Both freshening and cooling due to tilting was strongest in the FTZ, indicating that it is a critical zone for BL and TI formation through the tilting process. In addition, the salinity gradient was the dominant contributor to the horizontal density gradient during both cruises, which corroborates the formation of BLs and TIs via the tilting mechanism. DO within BLs showed almost the same or higher values compared to that found within the overlying mixed layer, further confirming that BLs and TIs are formed through surface processes and hence that the tilting of the SSS front is largely in response to the surface flow.

The distribution of BLs and TIs during the two SPURS-2 cruises was mostly consistent with the seasonal climatology of KS2020. The results largely support KS2020's idea that BLs and TIs are formed by tilting of the SSS front in boreal summer and autumn and that precipitation is also important for the BL formation in boreal summer. On the other hand, some new insights into BL and TI formation are obtained from the results of this study. During both the 2016 and 2017cruises, surface freshening and cooling by tilting showed a very patchy and/or porous distribution (Figs. 11 and 12) compared to the distribution of BLs and TIs (Figs. 4 and 6). This is in contrast to the continuous distribution of Ekman freshening along the SSS front found in the climatological study by KS2020. This implies that the BL and TI formation through the tilting mechanism occurs only intermittently and on much faster time scales than resolved by KS2020. At the same time, the patchiness and porosity in the distribution of BLs and TIs implies that their destruction can also occur as a result of destabilization by wind mixing and/or evaporation. This patchiness and porosity in the distribution of BLs and TIs can dampen the overall effect of BL and TI presence in reducing heat exchange through entrainment or through air-sea interaction. To better assess the impact of BLs and TIs on the entrainment process and air-sea interaction, time-series observations such as from moorings, will be important in future studies.

During the 2016 summer cruise, although freshening and cooling by tilting was strong in the FTZ, the freshening and cooling by Ekman advection was weak. Similarly, during the 2017 autumn cruise, freshening attributed to tilting was strong in the EPFP and the FTZ, while the freshening by Ekman advection was weak. Cooling by tilting in the FTZ was also distinct from the weak cooling by Ekman advection. These results imply that the surface geostrophic flow has an important role in the tilting of the SSS front and hence in the formation of BLs and TIs on synoptic scales, especially in the FTZ. This is in contrast to KS2020, who found that on seasonal time scales, Ekman advection acted alone to freshen and cool the surface layer, contributing to the formation of BLs with TIs through the tilting of the SSS front in boreal summer and autumn.

729 The eastward NECC is the prevailing current in the EPFP, but meridional perturbations in
730 the NECC flow such as from small meanders, mesoscale eddies and/or tropical instability waves
731 and filaments, may cross and tilt the SSS front contributing to BL and TI formation, such as
732 shown in the modelling study by Bingham et al. (2020). Unfortunately, our SPURS-2
733 observations were mainly oriented north-south and so we are unable to estimate the vertical shear
734 of the meridional geostrophic flow without transect observations in the zonal direction. Thus, we
735 cannot fully understand how the geostrophic flow in the meridionally-meandering NECC might
736 contribute to the vertical sheared velocity in the meridional direction. Similarly, we can only
737 estimate the meridional component of Ekman advection and its contribution to the tilting process
738 as the SPURS-2 observations lack sufficient resolution in the zonal direction (see Figure 3).
739 Although the zonal gradient of SSS and SST is much smaller than the meridional gradient (e.g.,
740 Figs. 4 and 6), the strong eastward NECC can also potentially contribute to BL and TI formation
741 through the tilting process and so compensate for the small zonal gradient of SSS and SST to
742 potentially result in surface freshening and cooling. Studies using high-resolution ocean models
743 will be important to further pursue the small spatio-temporal scale formation of BLs and TIs in
744 the eastern Pacific as well as any contribution to their formation by the NECC.

745 **Acknowledgments**

746 SK is supported by JSPS Overseas Research Fellowships. JS and SK are supported by
747 NASA Grant Number 80NSSC18K1500. FB's work on SPURS-2 was supported by NASA
748 grant NNX15AF72G, and by the Jet Propulsion Laboratory through the Salinity Continuity
749 Processing activity. The authors are thankful to an anonymous reviewer for their valuable and
750 constructive comments. The SPURS-2 uCTD and CTD data collected and reported on in this
751 manuscript were supported through NNX15AF67G to JS. The Argo float data used in this study
752 were collected and made freely available by the International Argo Project and the national
753 programs that contribute to it (http://www.argo.ucsd.edu; http://www.jcommops.org/argo). Argo
754 is a pilot program of the Global Ocean Observing System. The Argo profiles were from the
755 Argo Global Data Assembly Center (ftp://usgodae.org/pub/outgoing/argo;
756 ftp://ftp.ifremer.fr/ifremer/argo) and Advanced automatic QC Argo data version 1.2. by the
757 Japan Agency for Marine-Earth Science and Technology (see
758 http://www.jamstec.go.jp/ARGO/argo_web/argo/?page_id=100&lang=en). The L3 70-km
759 version-4.0 product of the NASA Soil Moisture Active Passive was provided by NASA's
760 Physical Oceanography Distributed Active Archive Center (PO.DAAC;
761 https://podaac.jpl.nasa.gov/dataset/SMAP_RSS_L3_SSS_SMI_MONTHLY_V4). The
762 Advanced Very High Resolution Radiometer product OISST was provided by the National
763 Oceanic and Atmospheric Administration (NOAA) National Centers for Environmental
764 Information (https://www.ncdc.noaa.gov/oisst). The uCTD, CTD, and ADCP profiles from the
765 SPURS-2 cruises are available from the PO.DACC SPURS-2 webpage (https://podaac-
766 tools.jpl.nasa.gov/drive/files/allData/insitu/L2/spurs2/). The authors are thankful to Drs. Carol
767 Anne Clayson and James Edson for shipboard wind and precipitation data from the SPURS-2
768 cruises, which are also available at the PO.DAAC SPURS-2 webpage. Information on the
769 shipboard ADCP data acquisition, processing, and distribution is found at the UHDAS site
770 (http://currents.soest.hawaii.edu/docs/ adcp_doc/index.html). IMERG data were obtained from
771 the NASA Goddard Earth Sciences Data and Information Services Center
772 (https://disc.gsfc.nasa.gov/datasets/GPM_3IMERGDF_06/summary?keywords=%22IMERG%2
773 0final%22).

References

Akima, H. (1970). A new method of interpolation and smooth curve fitting based on local procedures. *Journal of the ACM (JACM)*, 17(4),589–602. https://doi.org/10.1145/321607.321609

Alory, G., Maes, C., Delcroix, T., Reul, N., & Illig, S. (2012). Seasonal dynamics of sea surface salinity off Panama: The far eastern Pacific fresh pool. *Journal of Geophysical Research*, 117, C04028. https://doi.org/10.1029/2011JC007802

Amador, J. A., Alfaro, E. J., Lizano, O. G., & Magaña, V. O. (2006). Atmospheric forcing of the Eastern Tropical Pacific: A review. *Progress in Oceanography*, 69(2-4), 101–142. https://doi.org/10.1016/j.pocean.2006.03.007

Benway, H. M., & Mix, A. C. (2004), Oxygen isotopes, upper-ocean salinity, and precipitation sources in the eastern tropical Pacific, *Earth and Planetary Science Letters*, 224(3-4), 493–507. https://doi.org/10.1016/j.epsl.2004.05.014

Bingham, F.M., Z. Li, S. Katsura & J. Sprintall (2020), Barrier Layers in a High-resolution Model in the Eastern Tropical Pacific, *Journal of Geophysical Research Oceans*, in press.

Bingham, F.M., Tsontos, V., deCharon, A., Lauter, C. J., & Taylor, L. (2019). The SPURS-2 east- ern tropical Pacific field campaign data collection. *Oceanography*, 32(2), 142–149, https://doi.org/10.5670/ oceanog.2019.222

Clayson, C. A., Edson, J. B., Paget, A., Graham, R., & Greenwood, B. (2019). The effects of rainfall on the atmosphere and ocean during SPURS-2. *Oceanography*, 32(2), 86–97. https://doi.org/10.5670/oceanog.2019.216

Cronin, M. F., & McPhaden, M. J. (2002). Barrier layer formation during westerly wind bursts. *Journal of Geophysical Research: Oceans*, 107(C12), 8020. https://doi.org/10.1029/2001JC001171

de Boyer Montégut, C., Mignot, J., Lazar, A., & Cravatte, S. (2007). Control of salinity on the mixed layer depth in the world ocean: 1.General description. *Journal of Geophysical Research*, 112, C06011. https://doi.org/10.1029/2006JC003953

Delcroix, T., & Hénin, C. (1991). Seasonal and interannual variations of sea surface salinity in the tropical Pacific Ocean. *Journal of Geophysical Research*, 96, 22,135–22,150. https://doi.org/10.1029/91JC02124.

Drushka, K., Sprintall, J., & Gille, S. T. (2014). Subseasonal variations in salinity and barrier-layer thickness in the eastern equatorial Indian Ocean. *Journal of Geophysical Research: Oceans*, 119, 805–823. https://doi.org/10.1002/2013JC009422

Edson, J. B., Jampana, V., Weller, R. A., Bigorre, S. P., Plueddemann, A. J., Fairall, C. W., et al. (2013). On the exchange of momentum over the open ocean. *Journal of Physical Oceanography*, 43(8), 1589–1610. https://doi.org/10.1175/JPO-D-12-0173.1

Fairall, C., Bradley, E. F., Hare, J., Grachev, A., & Edson, J. (2003). Bulk parameterization of air-sea fluxes: Updates and verification for the COARE algorithm. *Journal of Climate*, 16(4), 571–591. https://doi.org/10.1175/1520-0442(2003)016<0571:BPOASF>2.0.CO;2

814 Fiedler, P. C., & Talley, L. D. (2006). Hydrography of the eastern tropical Pacific: A review.
815 *Progress in Oceanography*, 69(2–4), 143–180.
816 https://doi.org/10.1016/j.pocean.2006.03.008

817 Godfrey, J. S., & Lindstrom, E. J. (1989), The heat budget of the equatorial western Pacific
818 surface mixed layer, *Journal of Geophysical Research*, 94(C6), 8007–8017

819 Guimbard, S., Reul, N., Chapron, B., Umbert, M., & Maes, C. (2017). Seasonal and interannual
820 variability of the Eastern Tropical Pacific Fresh Pool. *Journal of Geophysical Research:*
821 *Oceans*, 122, 1749–1771. https://doi.org/10.1002/2016JC012130

822 Hayward, T. L. (1994), The shallow oxygen maximum layer and primary production, *Deep Sea*
823 *Research Part I*, 41(3), 559–574. https://doi.org/10.1016/0967-0637(94)90095-7

824 Jenkins, W. J., & Goldman, J. C. (1985). Seasonal oxygen cycling and primary production in the
825 Sargasso Sea. *Journal of Marine Research*, 43(2), 465–491.
826 https://doi.org/10.1357/002224085788438702

827 Kao, H.-Y., & Lagerloef, G. S. E. (2015). Salinity fronts in the tropical Pacific Ocean. *Journal of*
828 *Geophysical Research: Oceans*, 120, 1096–1106. https://doi.org/10.1002/2014JC010114

829 Katsura, S. & Sprintall, J. (2020). Seasonality and Formation of Barrier Layers and Associated
830 Temperature Inversions in the Eastern Tropical North Pacific. *Journal of Physical*
831 *Oceanography*, 50, 791-808. https://doi.org/10.1175/JPO-D-19-0194.1

832 Katsura S., Oka, E., & Sato, K. (2015). Formation Mechanism of Barrier Layer in the
833 Subtropical Pacific. *Journal of Physical Oceanography*, 45, 2790-2805.
834 https://doi.org/10.1175/JPO-D-15-0028.1

835 Katsura, S., Oka, E., Qiu, B., & Schneider, N. (2013). Formation and subduction of North Pacific
836 Tropical Water and their interannual variability. *Journal of Physical Oceanography*,
837 43(11), 2400–2415. https://doi.org/10.1175/JPO-D-13-031.1

838 Kummerow, C. (1998). Beamfilling errors in passive microwave rainfall retrievals, Journal of
839 Applied Meteorology, 37(4), 356–370. https://doi.org/10.1175/1520-
840 0450(1998)037<0356:BEIPMR>2.0.CO;2

841 Lagerloef, G., Schmitt, R., Schanze, J., & Kao, H.-Y. (2010). The ocean and the global water
842 cycle. *Oceanography*, 23(4), 82–93. https://doi.org/10.5670/oceanog.2010.07

843 Li, L., Schmitt, R. W., Ummenhofer, C. C., & Karnauskas, K. B. (2016a). Implications of North
844 Atlantic sea surface salinity for summer precipitation over the US Midwest: Mechanisms
845 and predictive values. *J. Climate*, **29**, 3143-3159

846 Li, L., Schmitt, R. W., Ummenhofer, C. C., & Karnauskas, K. B. (2016b). North Atlantic salinity
847 as a predictor of Sahel rainfall. *Science Advances*, **2**, e1501588

848 Li, Y., Han, W., Ravichandran, M., Wang, W., Shinoda, T., & Lee, T. (2017a). Bay of Bengal
849 salinity stratification and Indian summer monsoon intraseasonal oscillation: 1.
850 Intraseasonal variability and causes. *Journal of Geophysical Research: Oceans*, 122,
851 4291–4311, doi:10.1002/2017JC012691.

852 Li, Y., Han, W., Wang, W., Ravichandran, M., Lee, T., & Shinoda, T. (2017b). Bay of Bengal
853 salinity stratification and Indian summer monsoon intraseasonal oscillation: 2. Impact on

SST and convection. *Journal of Geophysical Research: Oceans*, 122, 4312–4328, doi:10.1002/2017JC012692.

Lindstrom, E., Bryan, F., & Schmitt, R. (2015). SPURS: Salinity processes in the upper-ocean regional study: The North Atlantic experiment. *Oceanography*, 28(1), 14–19. https://doi.org/10.5670/oceanog.2015.01

Lindstrom, E. J., Edson, J. B., Schanze, J. J., & Shcherbina, A. Y. (2019). SPURS-2: Salinity Processes in the Upper-ocean Regional Study 2.The eastern equatorial Pacific experiment. *Oceanography*, 32(2), 15–19. https://doi.org/10.5670/oceanog.2019.207

Maes, C., Picaut, J., & Belamari, S. (2002). Salinity barrier layer and onset of El Nino in a Pacific coupled model. *Geophysical Research Letters*, 29, 2206. https://doi.org/10.1029/2002GL016029

Maes, C., Picaut, J., & Belamari, S. (2005). Importance of salinity barrier layer forth e buildup of El Niño. *Journal of Climate*, 18, 104–118. https://doi.org/10.1175/JCLI-3214.1

Mignot, J., de Boyer Montégut, C., & Tomczak, M. (2009). On the porosity of barrier layers. *Ocean Science*, 5(3), 379–387. https://doi.org/10.5194/os-5-379-2009

Mignot, J., Lazar, A., & Lacarra, M. (2012). On the formation of barrier layers and associated vertical temperature inversions: A focus on the northwestern tropical Atlantic. *Journal of Geophysical Research*, 117, C02010. https://doi.org/10.1029/2011JC007435

Meissner, T. & Wentz, F. J. (2018). RSS SMAP Level 3 Sea Surface Salinity Standard Mapped Image 8-Day Running Mean V4.0 Validated Dataset. Ver. 4.0. *PO.DAAC*, accessed 23 Sep 2019, https://doi.org/10.5067/SMP3A-3SMCS.

Melnichenko, O., Hacker, P., Bingham, F.M., & Lee, T. (2019). Patterns of SSS variability in the east- ern tropical Pacific: Intraseasonal to interannual timescales from seven years of NASA satellite data. *Oceanography*, 32(2), 20–29, https://doi.org/10.5670/oceanog.2019.208

Mignot, J., Lazar, A., & Lacarra, M. (2012). On the formation of barrier layers and associated vertical temperature inversions: A focus on the northwestern tropical Atlantic. *Journal of Geophysical Research*, 117, C02010. https://doi.org/10.1029/2011JC007435

Najjar, R. G., & Keeling, R. F. (1997). Analysis of the mean annual cycle of the dissolved oxygen anomaly in the World Ocean. *Journal of Marine Research*, 55(1), 117–151. https://doi.org/10.1357/0022240973224481

Oka, E., Talley, L. D., & Suga, T. (2007). Temporal variability of winter mixed layer in the mid- to high-latitude North Pacific. *Journal of Oceanography*, 63(2), 293–307. https://doi.org/10.1007/s10872-007-0029-2

Pujiana, K., & McPhaden, M. J. (2018). ocean surface layer response to convectively coupled Kelvin waves in the Eastern Equatorial Indian Ocean. *Journal of Geophysical Research: Oceans*, 123, 5727–5741. https://doi.org/10.1029/2018JC013858

Rathore, S., Bindoff, N. L., Ummenhofer, C.C., Phillips, H. E., & Feng, M. (2020). Near-Surface Salinity Reveals the Oceanic Sources of Moisture for Australian Precipitation through Atmospheric Moisture Transport. *Journal of Climate*, 33, 6707–6730. https://doi.org/10.1175/JCLI-D-19-0579.1

Reid, J. L., Jr. (1962). Distribution of dissolved oxygen in the summer thermocline. *Journal of Marine Research*, 20,138 –148.

Ren, L., & Riser, S. C. (2009). Seasonal salt budget in the northeast Pacific Ocean. *Journal of Geophysical Research*, 114, C12004. https://doi.org/10.1029/2009JC005307

Reynolds, R. W., Smith, T. M., Liu, C., Chelton, D. B., Casey, K. S., & Schlax, M. G. (2007). Daily high-resolution-blended analyses for seasurface temperature. *Journal of Climate*, 20(22), 5473–5496. https://doi.org/10.1175/2007JCLI1824.1

Roemmich, D., Morris, M., Young, W. R., & Donguy, J. R. (1994). Fresh equatorial jets. *Journal of Physical Oceanography*, 24(3), 540–558. https://doi.org/10.1175/1520-0485(1994)024<0540:FEJ>2.0.CO;2

Sato, K., Suga, T., & Hanawa, K. (2004), Barrier layer in the North Pacific subtropical gyre. *Geophysical Research Letters*, 31, L05301. doi:10.1029/2003GL018590

Sato, K., Suga, T., & Hanawa, K. (2006). Barrier layers in the subtropical gyres of the world's oceans. *Geophysical Research Letters*, 33,L08603. https://doi.org/10.1029/2005GL025631

Schmitt, R. W. (2008). Salinity and the global water cycle. *Oceanography*, 21(1), 12–19. https://doi.org/10.5670/oceanog.2008.63.

Skofronick-Jackson, G., Petersen, W.A., Berg, W., Kidd, C., Stocker, E.F., Kirschbaum, D.B., Kakar, R., Braun, S.A., Huffman, G.J., Iguchi, T., Kirstetter, P.E., Kummerow, C., Meneghini, R., Oki, R., Olson, W.S., Takayabu, Y.N., Furukawa, K., & Wilheit, T. (2017). The Global Precipitation Measurement (GPM) Mission for Science and Society. *Bulletin of the American Meteorological Society*, 98, 1679–1695, https://doi.org/10.1175/BAMS-D-15-00306.1

Sprintall, J. (2019). Upper ocean salinity stratification during SPURS-2. *Oceanography*, 32(2), 40–41, https://doi.org/10.5670/oceanog.2019.210.

Sprintall, J., & Tomczak, M. (1992). Evidence of the barrier layer in the surface layer of the tropics. *Journal of Geophysical Research*, 97(C5), 7305–7316. https://doi.org/10.1029/92JC00407

Suga, T., Motoki, K., Aoki, Y., & MacDonald, A.M. (2004). The North Pacific climatology of winter mixed layer and mode waters. *Journal of Physical Oceanography*, 34, 3–22. https://doi.org/10.1175/1520-0485(2004)034<0003:TNPCOW>2.0.CO;2

Sukigara, C., Suga, T., Saino, T., Toyama, K., Yanagimoto, D., Hanawa, K., & Shikama, N. (2011). Biogeochemical evidence of large diapycnal diffusivity associated with the subtropical mode water of the North Pacific. *Journal of Oceanography*, 67(1), 77–85. https://doi.org/10.1007/s10872-011-0008-5

Tippins, D., & Tomczak, M. (2003). Meridional Turner angles and density compensation in the upper ocean, *Ocean Dynamics*, 53, 332–342, doi:10.1007/s10236-003-0056-5.

Ullman, D. S., & Hebert., D. (2014). Processing of Underway CTD Data, *Journal of tmospheric and Oceanic Technology*, 31, 984–998, doi:10.1175/JTECH-D-13-00200.1.

Vialard, J., & Delecluse, P. (1998). An OGCM study for the TOGA decade. Part I: Role of salinity in the physics of the western Pacific fresh pool. *Journal of Physical Oceanography*, 28(6), 1071–1088.

Waliser, D. E., & Gautier, C. (1993). A satellite-derived climatology of the ITCZ. *Journal of Climate*, 6(11), 2162–2174. https://doi.org/10.1175/1520-0442(1993)006<2162:ASDCOT>2.0.CO;2

Yan, Y., Li, L., & Wang, C. (2017). The effects of oceanic barrier layer on the upper ocean response to tropical cyclones. *Journal of Geophysical Research: Oceans*, 112, 4829–4844. https://doi.org/10.1002/2017JC012694

Yu, L. (2014), Coherent evidence from Aquarius and Argo for the existence of a shallow low-salinity convergence zone beneath the Pacific ITCZ, *Journal of Geophysical Research: Oceans*, 119, 7625–7644, doi:10.1002/2014JC010030

Yu, L. (2015). Sea-surface salinity fronts and associated salinity-minimum zones in the tropical ocean. *Journal of Geophysical Research: Oceans*, 120, 4205–4225. https://doi.org/10.1002/2015JC010790